Flow and Double-Diffusive Instability in Porous Media

By

Joseph Ntahompagaze (joseph.ntahompagaze@aims.edu.gh)

June 2014

A RESEARCH PROJECT PRESENTED TO AIMS-GHANA IN PARTIAL FULFILMENT OF THE REQUIREMENTS FOR THE AWARD OF MASTER OF SCIENCE IN MATHEMATICAL SCIENCES

DECLARATION

This work was carried out at AIMS-Ghana in partial fulfilment of the requirements for a Master of Science Degree.

I hereby declare that except where due acknowledgement is made, this work has never been presented wholly or in part for the award of a degree at AIMS-Ghana or any other University.

Student: Joseph Ntahompagaze 

Supervisor: Dr. David Pritchard 

ACKNOWLEDGEMENTS

This is an opportunity for me to say thank you to my supervisor Dr. David Pritchard for his support and advice to carry out this thesis as well as my tutor Augustine Larweh Mahu for his advice. I also thank the English language teacher, Beauty Beatrice Kwawu for her proofreading and advice during the writing of the work. I thank the University of Rwanda, especially the College of Science and Technology for allowing me to come to pursue Master's studies at AIMS-Ghana. Many thanks also go to my darling wife Nyiransabimana Esperance, my father Havugimana and my mother Nyirabashyitsi for their moral support during my studies.

DEDICATION

This work is dedicated to my son Mugabwa Christian.

Abstract

The flow and double-diffusive instability in porous media has been studied in this work. The linear perturbation theory has been utilised for both thermal convection and double-diffusive convection. We found that for the thermal convection, below the critical Rayleigh number, the system is stable and above that number the system is unstable. For the double-diffusive convection, the stability transition has two different behaviour: when the concentration gradient is negative, the perturbations are in exponential form. When it is positive, we observe the oscillatory mode. The weakly non-linear stability analysis has been studied using the Galerkin approximation approach and we found that for different values of Rayleigh number, the solutions bifurcate. Using numerical simulations, we found that when the base state is unstable, the perturbations do not grow forever but saturate at a finite amplitude; however the finite-amplitude solution is not a global attractor.

Contents

1. Introduction and Literature Review

1.1 Introduction

Double-diffusive convection in a porous medium is interesting from both physical and mathematical standpoints. Physically, it is applied in the different area of geology and engineering. Mamou and Vasseur (1999) and Pritchard and Richardson (2007) listed areas where double-diffusive convection is applied: some of these are contaminant transport in saturated soil, underground disposal of nuclear waste, heat transfer in geothermal reservoirs, in electro-chemical and drying processes. Mathematically, it involves a variety of bifurcation structures and transitions to instability where numerical simulations must be used to predict the amplitude of the bifurcated solutions.

In this work, we intend to illustrate how flow responds to the perturbations of temperature for thermal convection, and how flow responds to the perturbations of temperature and salt concentration for double-diffusive convection. We will use both linear perturbation theory and a weakly non-linear approximation method.

The work is organised as follows: in section two of chapter one, we review the background of the double-diffusive convection problem and state some types of bifurcations. In chapter two, we describe the governing equations, including Darcy's law, the continuity equation and transport equations for heat and salinity. The third chapter examines the thermal convection by considering the Horton-Rogers-Lapwood problem, where the linear perturbation theory has been introduced leading to linear stability analysis. We describe the competition of both thermal diffusion and viscosity against buoyancy force in the thermal instability. In chapter four, we focus on the main problem of double-diffusive convection using the linear stability analysis, where the thermal gradient and salt concentration gradient may be in competition. After linear analysis, the weakly non-linear problem is studied using the Galerkin approximation approach to investigate whether the perturbations would grow forever or would be saturated at finite amplitudes. We use numerical simulations to see the behaviour of the solutions. Finally in chapter five, we highlight and summarise the work done so far.

1.2 Literature Review

Natural convection is the motion of a fluid without external effects applied to it, except the gravitational force. Usually natural convection is caused by an applied temperature gradient which makes the fluid density different in different places (Corson, 2012). The fluid near the hot area becomes hot and less dense compared to the rest however it will rise. When it is moving away from the hot area, the surrounding cooler fluid, more dense than the hot fluid, also moves, approaching the hot boundary.

We have the fluid which is moving and it transports heat. There are two contributing phenomena to the transportation of heat; conduction and convection. Since diffusion occurs rapidly compared

to the convective motion, it tends to minimise the temperature difference. But convection occurs slowly due to the buoyancy effect. Charru (2011) stated that there is a destabilising phenomenon (buoyancy) and a stabilising one (thermal diffusion).

This phenomenon had become a point of interest when Benard in 1900, observed that the thermal instability occurring in a layer of a fluid heated from below. Sixteen years later, in 1916 Rayleigh developed a theoretical requirement for the convection of fluid to begin occurring in the layer of a fluid with free boundaries. He came up with a number which is proportional to the gravitational acceleration, thermal expansion of the fluid, vertical temperature gradient and inversely proportional to the kinematic viscosity of the fluid and the thermal diffusivity of the fluid. The number is called the Rayleigh number Ra. He showed that the temperature gradient has to be big enough so that the number exceeds a critical value for the instability to occur (Kundu et al., 2012).

The thermal instability in the porous medium was firstly studied by Horton and Rogers (1945). But instead of viscous fluid in the layer, they considered a porous medium saturated with a fluid of uniform composition. Three years later, Lapwood (1948) considered in more detail the instability analysis in a saturated porous medium. He found that the critical value for the Rayleigh number is $4\pi^2$ (Phillips, 2009).

The linear perturbation theory is used to determine the conditions under which convection occurs. We assume that the base state is at rest before being perturbed. Then the issue is to examine how the equations reveal the decay or growth of the perturbations. The disturbances are very small so that we neglect the higher order terms (Kundu et al., 2012).

In our dynamical stability analysis we deal with how the system responds to the temperature and flow perturbations. We say that the system is dynamically stable if once we perturb it, it is able to come back to its initial state (the disturbance dies away). Otherwise we say that the system is dynamically unstable.

Charru (2011) illustrated the fundamental techniques to investigate the linear stability of a base state in fluid flow. The first one is the derivation of the equations that govern the system under consideration for small disturbances of base state. The second one is to apply linearisation and determination of the normal modes, and then look for the dispersion relation. This relation connects the wave-vector and growth rate (Godreche and Manneville, 1998). We consider the linear equations to admit solutions that are exponential in space and in time. And the perturbations are assumed to be the superposition of these solutions which are evolving independently. Thus we may say that perturbations are normal modes due to the orthogonality of the sinusoidal functions. When we introduce these normal modes into the linear equations, we obtain an algebraic system whose determinant is required to vanish and from this condition, we obtain the dispersion relation which becomes a focus of the stability analysis.

The hydrodynamic instability that involves two gradients, usually temperature gradient and species concentration gradient, was first proposed by Stommel, Arons and Blanchard in 1956 (Turner, 1973). The detailed explanation of the problem was studied by Stern in 1960 (Kundu et al., 2012). The double-diffusive instability in porous medium was firstly studied by Nield in 1968 and it was called a 'thermohaline' phenomenon. He generalized the problem studied previously by Horton, Rogers and Lapwood (Nield and Bejan, 2006). In thermal convection the

density difference is produced only by the temperature gradient. But in thermohaline convection, the density difference depends on temperature and solute concentration.

Since we are dealing with instabilities, we will need the information about bifurcation from dynamical systems. When the system has a parameter for which when it varies, the behaviour of the solutions changes, we call this effect the bifurcation. The critical value of the parameters that corresponds to this change is called a bifurcation point (Drazin, 2002). There are different types of bifurcations. Here we are interested in the pitchfork bifurcation and saddle-node bifurcation. Strogatz (1994) stated that these kinds of bifurcations are common to physical problems that experience symmetry in their behaviour. We have two types of pitchfork bifurcations. The first one is called a supercritical pitchfork bifurcation. This kind of bifurcation may appear when one solution splits into more than one solutions after passing through the bifurcation point. The second one is a sub-critical pitchfork bifurcation where many solutions merge into one solution after passing through the bifurcation point. For a saddle-node bifurcation, more than one solution grow after a saddle-node point, where before that point there were no solution (See section 3 from Strogatz (1994) for more about these types of bifurcations).

2. Governing equations of fluid flow in porous media

In this section the equations that govern the flow of viscous fluid in a saturated porous medium, when temperature and salt are taken into account, are presented.

A porous medium is a material that contains empty spaces, called pores. This kind of medium has properties such as porosity and permeability. Porosity can be defined as the volume ratio between the volume of pores and the total volume of the material (Kumar, 2012). Permeability is the measure of the ability of a material to allow fluid to pass through. O'Brien et al. (2007) noted that there is a correlation between porosity and permeability. But this is an empirical result rather than the relation from the definition. In this work we will denote the permeability of the porous medium by K and porosity will be denoted by ϕ.

In this model, we assume that the porosity does not evolve with time. We assume also that the pores are much larger than the size of molecules in the fluid, but the pores are much smaller than the volume of the considered matrix. An example is the pores in sandstone which typically have a size of $0.1mm$ (Phillips, 2009). This allows us to treat the medium as a continuum.

2.1 Darcy's law

Darcy's law (Phillips 2009, section 2.4) is an equation that connects the flow rate, the pressure difference and the buoyancy term. This equation in a porous medium replaces the Navier-Stokes momentum equation. When the fluid is in motion the transport velocity $\overrightarrow{u}$ is given as

$$\overrightarrow{u} = -\frac{K}{\mu}\left(\overrightarrow{\nabla} p + \rho g \overrightarrow{k}\right), \tag{2.1.1}$$

where K is the permeability of the medium and μ is the viscosity of the fluid and $\overrightarrow{k}$ is the unit vector in the upward direction. According to Phillips (2009, section 4.2), the density is related to the temperature T and the salinity S (see section 2.3) and reference density ρ_0 by

$$\rho = \rho_0(1 - \alpha T + \beta S), \tag{2.1.2}$$

where ρ_0 is the reference density, α is the thermal expansion and β the salinity expansion. This linear model is valid for small changes in temperature T and in salinity S. When there is no salinity the density ρ reduces to

$$\rho = \rho_0(1 - \alpha T). \tag{2.1.3}$$

2.2 The continuity equation for mass balance

When a fluid is flowing the conservation of total mass must be considered. For incompressible fluid, where density stays the same, and when the porosity of the medium is constant, we have

$$\overrightarrow{\nabla}.\overrightarrow{u} = 0. \tag{2.2.1}$$

This is the mass conservation for incompressible fluid flow (Phillips 2009, section 2.3). This assumption that the fluid has a constant density in the continuity equation is called the Boussinesq approximation. In 1903, Boussinesq discussed an approximation which can be described as follows: when there is a small perturbation to the reference state, the pressure and density will be affected. However the small changes in the density cause only very small corrections in the inertial properties of the fluid. These corrections are neglected since they are small. The same small changes in the density also affect the buoyancy and this effect cannot be neglected (see equations (2.1.2) and (2.1.3)). The same approximation applies for other fluid properties like viscosity and diffusion (Turner, 1973). In this work we will treat the fluid as being of constant density except in the buoyancy term ρg which drives the convection.

2.3 Transport equations for heat and for dissolved chemical species (salinity)

In the saturated porous medium, heat can be transported through both the matrix and the fluid present in the pores. The salt can diffuse only through the fluid in the pores. Additionally when the fluid is flowing the temperature and the salt may also be transported.

2.3.1 Thermal energy balance equation.

The transport of heat in the fluid can be expressed in terms of the heat balance. We consider a system which contains matrix and flowing fluid. The matrix has specific heat capacity C_{sM} and density ρ_M, while the fluid has the specific heat capacity C_{sF} and the density ρ_F.

When there is no heat source present in the system, we can write the energy balance equation as

$$M\frac{\partial T}{\partial t} + \overrightarrow{u}.\overrightarrow{\nabla}T = \kappa\nabla^2 T. \tag{2.3.1}$$

This is known as the thermal energy balance equation (Phillips 2009, section 2.7). Here T is the temperature, $\overrightarrow{u}$ is the velocity of fluid flow, $M = \frac{(\rho C)_M}{(\rho C)_F}$ is the matrix-to-fluid heat capacity ratio and the thermal diffusivity $\kappa = \frac{\kappa_M}{(\rho C)_F}$ is the ratio between thermal conductivity of saturated medium and heat capacity of the fluid.

2.3.2 Dissolved species balance equation.

We still have the same system composed by the matrix with porosity ϕ and the homogeneous fluid with density ρ. When salt diffusion process is occurring, we consider the effect to be in

spatial distribution, so that the concentration will change in space and in time. In this context we define the concentration c as mass of dissolved solute per unit volume of solution, rather than per unit mass (Phillips, 2009). We define the salinity S as the ratio between concentration c and density ρ,

$$S = \frac{c}{\rho}. \tag{2.3.2}$$

Now the balance equation defining the process in the system is described by the equation

$$\frac{\partial S}{\partial t} + \overline{v}.\overrightarrow{\nabla} S = D\nabla^2 S. \tag{2.3.3}$$

This is known as the dissolved species balance equation (Phillips 2009, section 2.8). Here, S is the salinity, D is the macroscopic dispersion coefficient and the mean fluid velocity $\overline{v}$ is a ratio between the transport velocity $\overrightarrow{u}$ to porosity ϕ. The above equation can be written as

$$\phi\frac{\partial S}{\partial t} + \overrightarrow{u}.\overrightarrow{\nabla} S = \phi D\nabla^2 S. \tag{2.3.4}$$

This is the dissolved species balance equation which will be considered in the rest of this work. It is important to note that the salt diffusion D is much smaller than the thermal diffusion κ.

Phillips (2009) listed several factors that cause the salt to diffuse slowly in water. The first one is that the porosity is less than one $(\phi < 1)$. The second is, there is small molecular diffusivity of salt on water. The last one is that the pathways made by pores are not linear, but sinuous.

3. Horton-Rogers-Lapwood problem (Rayleigh-Darcy instability)

Consider the Figure 3.1, the porous layer has height h, the temperature decreases in the upward $z-$direction. It is heated from below and cooled from the top. The instability for the porous layer heated from below and cooled from above, is known as the Horton-Rogers-Lapwood problem. It was first discussed by Horton and Rogers (1945) and later in 1948, Lapwood explained this problem in more detail (Lapwood, 1948). In this chapter, the linear perturbation theory is used to investigate this problem.

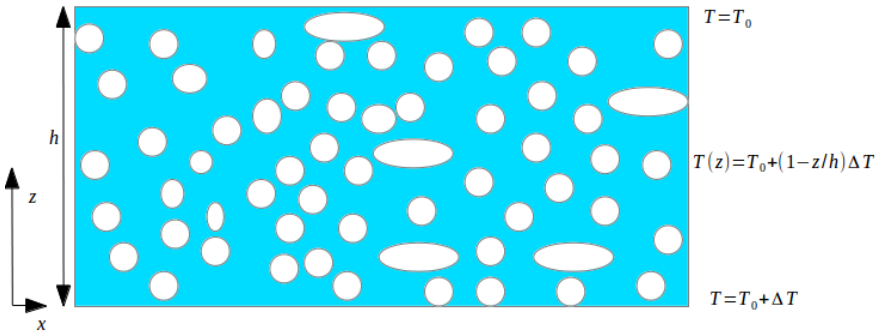

Figure 3.1: A sketch for porous layer of height h, the blue color represents water, white circles represent sandstone. Temperature is high at the bottom and low at the top.

The top of the layer is cooler than the bottom. The mathematics behind this situation is derived by considering the governing equations (2.1.1), (2.1.3), (2.2.1) and (2.3.1) which are Darcy's law, mass conservation for incompressible flows, and thermal energy balance respectively. We are introducing linear perturbation theory in section 3.1 to analyse the problem presented here.

If we define the velocity vector $\overrightarrow{u} = (u, v, w)$ and $\overrightarrow{\nabla}_H = \overrightarrow{i}\frac{\partial}{\partial x} + \overrightarrow{j}\frac{\partial}{\partial y}$ to be the horizontal gradient operator then we can write equation (2.1.1) as

$$\begin{aligned} \overrightarrow{\nabla}_H p &= -\frac{\mu}{K}\overrightarrow{u}_H, \\ \frac{\partial p}{\partial z} &= -\frac{\mu}{K}w - \rho g. \end{aligned} \tag{3.0.1}$$

Consider a saturated porous layer with thickness h which is heated from below. The fluid at the bottom possesses higher temperature than the fluid near the top. This results in a smaller density at the bottom than at the top. The fluid at the bottom will tend to move up by buoyancy. The diffusion will influence the hot molecules to diffuse away due to temperature difference and viscosity will also resist the motion. Hence instability will occur if the buoyancy is strong enough relative to viscosity and diffusion.

The temperature T_0 at the top of the layer is lower than the temperature at the bottom by a temperature difference ΔT. So the conditions at the boundaries are such that at the lower boundary : $z = 0$, $w = 0$ and $T = T_0 + \Delta T$, and the top boundary : $z = h$, $w = 0$ and $T = T_0$.

For steady state of rest: $u = v = w = 0$, $p = p_0(z)$, and $\frac{\partial p_0}{\partial z} = -\rho g$. For uniform temperature gradient, we have the following equality

$$\frac{dT}{dz} = -\frac{\Delta T}{h}. \tag{3.0.2}$$

Integrating this equation from bottom temperature $T_i = T_0 + \Delta T$ to temperature T, we have

$$T - T_i = -\frac{\Delta T}{h} z. \tag{3.0.3}$$

Substituting for the value of T_i, we have the temperature dependence on z, as

$$T = T_0 + \left(1 - \frac{z}{h}\right)\Delta T, \tag{3.0.4}$$

so that at $z = 0, T = T_0 + \Delta T$ while at $z = h, T = T_0$.

3.1 Perturbations of steady state of rest

The steady state is perturbed, with perturbations introduced in the velocity, temperature and pressure. The perturbations are small variations in space and in time. The quantities denoted with prime are small (and the prime does not indicate differentiation) since we are linearising about the basic state.

$$\overrightarrow{u} = 0 + \overrightarrow{u}'(x, y, z, t), \tag{3.1.1}$$

$$p = p_0(z) + p'(x, y, z, t), \tag{3.1.2}$$

$$T = T_0 + \left(1 - \frac{z}{h}\right)\Delta T + T'(x, y, z, t). \tag{3.1.3}$$

We have

$$\overrightarrow{\nabla}.\overrightarrow{u}' = 0. \tag{3.1.4}$$

Taking the horizontal gradient of $p = p_0(z) + p'(x, y, z, t)$, we have

$$\overrightarrow{\nabla}_H p = \overrightarrow{\nabla}_H p_0(z) + \overrightarrow{\nabla}_H p' = \overrightarrow{\nabla}_H p'. \tag{3.1.5}$$

This implies

$$\overrightarrow{\nabla}_H p' = -\frac{\mu}{K}\overrightarrow{u}'_H, \tag{3.1.6}$$

where $\overrightarrow{u}'_H = (u', v')$ is the vector composed by the horizontal components of the velocity $\overrightarrow{u}'$, which implies $\overrightarrow{u}' = \overrightarrow{u}'_H + w'\overrightarrow{k}$.

From $p = p_0(z) + p'(x, y, z, t)$, we have $p' = p - p_0$. Differentiating with respect to z, and using equations (3.0.1) and (3.1.2), we have

$$\frac{\partial p'}{\partial z} = -\frac{\mu}{K}w' - g\rho_0\left(1 - \alpha\left(T_0 + \left(1 - \frac{z}{h}\right)\Delta T\right)\right) + g\rho_0\alpha T' - \frac{\partial p_0}{\partial z}. \tag{3.1.7}$$

And using

$$\frac{\partial p_0}{\partial z} = -g\rho_0\Big(1 - \alpha(T_0 + (1 - \frac{z}{h})\Delta T)\Big), \tag{3.1.8}$$

we have

$$\frac{\partial p'}{\partial z} = -\frac{\mu}{K}w' + g\rho_0\alpha T'. \tag{3.1.9}$$

Equations (3.1.5) and (3.1.9) are combined to get

$$\overrightarrow{\nabla}p' = -\frac{\mu}{K}\overrightarrow{u}' + g\rho_0\alpha T'\overrightarrow{k}. \tag{3.1.10}$$

Taking the curl of equation (3.1.10) and using the result that $\overrightarrow{\nabla} \times (\overrightarrow{\nabla}p') = 0$, we have

$$\frac{\mu}{K}\overrightarrow{\nabla} \times \overrightarrow{u}' + g\rho_0\alpha\overrightarrow{\nabla} \times \Big(T'\overrightarrow{k}\Big) = 0. \tag{3.1.11}$$

By considering the equation (2.3.1) and introducing the perturbation from equations (3.1.1) and (3.1.3) and since only T' and $\overrightarrow{u}'$ are not constant, we have

$$M\frac{\partial T'}{\partial t} + \overrightarrow{u}'.\overrightarrow{\nabla}T' - \overrightarrow{u}'.\overrightarrow{\nabla}\Big(\frac{z\Delta T}{h}\Big) = \kappa\nabla^2 T'. \tag{3.1.12}$$

Expanding the third term on the left hand side of equation (3.1.12), we write

$$M\frac{\partial T'}{\partial t} + \overrightarrow{u}'.\overrightarrow{\nabla}T' - w'\frac{\Delta T}{h} = \kappa\nabla^2 T'. \tag{3.1.13}$$

Since $\overrightarrow{u}'.\overrightarrow{\nabla}T'$ is a product of small quantities, we can neglect it, so our set of equations becomes

$$M\frac{\partial T'}{\partial t} - w'\frac{\Delta T}{h} = \kappa\nabla^2 T'. \tag{3.1.14}$$

We consider only two-dimensional perturbations in the (x, z) plane, with zero velocity in the $y-$direction. In this context, components of the velocity can be defined in terms of a stream-function Ψ' as

$$u' = \frac{\partial \Psi'}{\partial z} \text{ and } w' = -\frac{\partial \Psi'}{\partial x}, \tag{3.1.15}$$

so that $\overrightarrow{\nabla}.\overrightarrow{u} = 0$ is automatically satisfied.

Now the differential equations (3.1.14) and (3.1.11) become

$$-\frac{\mu}{K}\left(\frac{\partial^2\Psi'}{\partial z^2} + \frac{\partial^2\Psi'}{\partial x^2}\right) - g\rho_0\alpha\frac{\partial T'}{\partial x} = 0, \tag{3.1.16}$$

and

$$M\frac{\partial T'}{\partial t} + \frac{\partial \Psi'}{\partial x}\frac{\Delta T}{h} = \kappa\nabla^2 T'. \tag{3.1.17}$$

We still have the boundary conditions that $T' = \frac{\partial\Psi'}{\partial x} = w' = 0$ at $z = 0$ and at $z = h$.

The differential equations (3.1.16) and (3.1.17) are linear, since there is no product of dependent variables. We consider the solution as a superposition of the Fourier modes which evolve independently. For sinusoidal imposed perturbations, we are looking for the separable solutions in the form

$$T' = \hat{T}\exp(ikx).\exp(nt)F(z) \text{ and } \Psi' = \hat{\Psi}\exp(ikx).\exp(nt)G(z), \tag{3.1.18}$$

where the coefficients $\hat{T}$ and $\hat{\Psi}$ are complex and we consider the real part to represent the physical quantities. The functions $F(z)$ and $G(z)$ are real functions without loss of generality.

If we are able to understand how these modes evolve, we can express n in terms of other parameters then we are able to identify the dominant term that can grow faster or decay faster, using the linear stability analysis.

We substitute the expressions of T' and that of Ψ' in equations (3.1.16) and (3.1.17), we have

$$-\frac{\mu}{K}\hat{\Psi}\left(-k^2G+\frac{d^2G}{dz^2}\right)-g\rho_0\alpha ik\hat{T}F=0, \tag{3.1.19}$$

and

$$Mn\hat{T}F+\frac{\Delta T}{h}ik\hat{\Psi}G=\kappa\left(-k^2F+\frac{d^2F}{dz^2}\right)\hat{T} \tag{3.1.20}$$

respectively.

The separation of variables gives us the two set of equations as

$$\frac{1}{F}\left(-k^2G+\frac{d^2G}{dz^2}\right)=\text{constant}, \tag{3.1.21}$$

$$\frac{G}{F}=\text{constant}, \tag{3.1.22}$$

and

$$\frac{1}{F}\left(-k^2F+\frac{d^2F}{dz^2}\right)=\text{constant}. \tag{3.1.23}$$

Without loss of generality, we take $G=F$ and then we write

$$\frac{1}{G}\left(-k^2G+\frac{d^2G}{dz^2}\right)=\text{constant}. \tag{3.1.24}$$

Considering the real solutions of equation (3.1.24), we have

$$G(z)=A\sin(mz)+B\cos(mz)=F(z), \text{ for some } m\in\mathbb{R}. \tag{3.1.25}$$

Using the boundary conditions which apply only to real variables, we have that

$$\text{Re}\left(\hat{T}F(z)\exp(ikx+nt)\right)=0 \text{ at } z=0, \text{ which implies that } F(0)=0, \text{ hence } B=0, \tag{3.1.26}$$

and

$$\text{Re}\left(\hat{T}F(z)\exp\left(ikx+nt\right)\right)=0 \text{ at } z=h, \Longleftrightarrow F(h)=0, \text{ hence } m=\frac{m^*\pi}{h} \text{ for some } m^*\in\mathbb{Z}. \tag{3.1.27}$$

Then we write temperature T' as

$$T'=A\sin\left(\frac{m^*\pi z}{h}\right)\exp\left(ikx+nt\right). \tag{3.1.28}$$

These boundary conditions are also satisfied for Ψ' and we write it with a different constant as

$$\Psi'=B\sin\left(\frac{m^*\pi z}{h}\right)\exp\left(ikx+nt\right). \tag{3.1.29}$$

At this stage we introduce the dimensionless quantities k^*, m^{**} and n^* defined by $m^{**}=m^*h$ so that $m^*=\frac{m^{**}}{h}$, $k^*=kh$ so that $k=\frac{k^*}{h}$ and $n^*=\frac{h^2Mn}{\kappa}$ so that $n=\frac{n^*\kappa}{h^2M}$. This implies that the solutions in equations (3.1.28) and (3.1.29) are updated to be

$$T'=A\sin\left(\frac{m^{**}\pi z}{h}\right)\exp\left(i\frac{k^*}{h}x+\frac{n^*\kappa}{h^2M}t\right) \text{ and } \Psi'=B\sin\left(\frac{m^{**}\pi z}{h}\right)\exp\left(i\frac{k^*}{h}x+\frac{n^*\kappa}{h^2M}t\right). \tag{3.1.30}$$

Putting T' and Ψ' in equation (3.1.16), and rearranging, simplifying the sinusoidal and exponential terms, we have

$$\frac{\mu}{K}\left(\frac{k^{*2}}{h^2}+\frac{m^{**2}\pi^2}{h^2}\right)B-g\rho_0\alpha\frac{ik^*}{h}A=0. \tag{3.1.31}$$

Putting T' and Ψ' in equation (3.1.17), and simplifying the similar terms, after rearranging, we have

$$\frac{ik^*}{h}\frac{\Delta T}{h}B+\left(\frac{n^*\kappa}{h^2}+\kappa\frac{k^{*2}}{h^2}+\kappa\frac{m^{**2}\pi^2}{h^2}\right)A=0. \tag{3.1.32}$$

Considering equation (3.1.31) and equation (3.1.32) simultaneously, we can use the determinant which is required to vanish so that we have non-trivial solution. Thus, we have

$$\begin{vmatrix} \frac{\mu}{K}\left(\frac{k^{*2}}{h^2}+\frac{m^{**2}\pi^2}{h^2}\right) & -ig\rho_0\alpha\frac{k^*}{h} \\ \frac{ik^*}{h}\frac{\Delta T}{h} & \left(\frac{n^*\kappa}{h^2}+\kappa\frac{k^{*2}}{h^2}+\kappa\frac{m^{**2}\pi^2}{h^2}\right) \end{vmatrix}=0.$$

From this determinant we have

$$\frac{\mu}{K}\left(\frac{k^{*2}}{h^2}+\frac{m^{**2}\pi^2}{h^2}\right)\left(\frac{n^*\kappa}{h^2}+\kappa\frac{k^{*2}}{h^2}+\kappa\frac{m^{**2}\pi^2}{h^2}\right)-\frac{k^{*2}}{h^3}g\rho_0\alpha\Delta T=0. \tag{3.1.33}$$

Expanding the product and dividing both sides by $\frac{\mu}{h^4K}\left(k^{*2}+m^{**2}\pi^2\right)\kappa$, we have

$$n^*=\frac{k^{*2}}{(k^{*2}+m^{**2}\pi^2)}\frac{Kg\rho_0\alpha h\Delta T}{\kappa\mu}-(k^{*2}+m^{**2}\pi^2). \tag{3.1.34}$$

Using the relation between kinematic viscosity ν and dynamic viscosity μ, with the relation $\nu=\frac{\mu}{\rho_0}$, and rearranging, we have

$$n^*=\frac{k^{*2}}{(k^{*2}+m^{**2}\pi^2)}Ra-(k^{*2}+m^{**2}\pi^2), \tag{3.1.35}$$

where $Ra=\frac{Kg\alpha h\Delta T}{\kappa\nu}$ is known as the Rayleigh number (Phillips, 2009).

3.2 Critical conditions for instability

Since this number n^* is real, it can be negative or positive. When it is negative, $n^* < 0$, this tells us that the perturbations will die away as time goes to infinity. This means that the basic state is stable. When it is positive, $n^* > 0$, the perturbations will grow exponentially with time which means that the flow will experience instability. Now we need to know the critical value when $n^* = 0$, this will happen when $Ra = \frac{(k^{*2}+m^{**2}\pi^2)^2}{k^{*2}}$.

Let us define the function $Ra(k^*, m^{**})$ with variables k^* and m^{**} as

$$Ra(k^*, m^{**}) = \frac{(k^{*2} + m^{**2}\pi^2)^2}{k^{*2}}. \tag{3.2.1}$$

We need to minimise the function $Ra(k^*, m^{**})$ over integer values of m^{**} and over all real values of k^* by differentiating with respect to k^*. So we have

$$\frac{\partial Ra(k^*, m^{**})}{\partial k^*} = 2k^* - \frac{2m^{**4}\pi^4}{k^{*3}}. \tag{3.2.2}$$

Setting $\frac{\partial Ra}{\partial k^*} = 0$, we have

$$k^* - \frac{m^{**4}\pi^4}{k^{*3}} = 0. \tag{3.2.3}$$

This is implies that

$$k^* = m^{**}\pi. \tag{3.2.4}$$

Substituting this value of k^* into equation (3.2.1), we have

$$Ra(k^*, m^{**}) = 4m^{**2}\pi^2. \tag{3.2.5}$$

For minimum value of $m^{**} = 1$, we have

$$Ra(k^*, m^{**}) = Ra_{critical} = 4\pi^2 \approx 39.43, \tag{3.2.6}$$

(see section 6.1 from (Nield and Bejan, 2006)). The states with small perturbations that produce Rayleigh number $Ra \lesssim 39.43$ is stable. When the Rayleigh number exceeds the critical value the flow becomes unstable.

3.3 Temperature and stream-function solutions after linear stability analysis

We are interested in plotting the temperature distribution and the flow of the fluid. To do this we need to know the constants A and B in terms of the parameters under consideration.

The linear stability analysis discussed above shows that the critical value of the Rayleigh number is $4\pi^2$. Below this critical value of the Rayleigh number (with $n^* < 0$), the perturbations will decay. The perturbations above this critical number (with $n^* > 0$) will grow and the system

will be unstable. The vertical and horizontal wave-numbers were minimized to be $k^* = \pi$ and $m^{**} = 1$ respectively, for $n^* = 0$.

When we substitute these minimized values in equation (3.1.31) and work in units such that $A = 1$, we find B to be complex

$$B = g\alpha \frac{kh}{\nu 2\pi} i. \tag{3.3.1}$$

Using the expression for Ra we can write this coefficient as

$$B = (Ra) i \frac{\kappa}{2\pi \Delta T}. \tag{3.3.2}$$

Since the considered critical value of Ra is $4\pi^2$, then $B = i\frac{2\pi\kappa}{\Delta T}$. Substituting A and B in equation (3.1.28) and (3.1.29), and decomposing the exponentials after setting $n^* = 0$ for marginal state, we have

$$T' = \sin\left(\frac{\pi z}{h}\right)\left(\cos\left(\frac{\pi x}{h}\right) + i\sin\left(\frac{\pi x}{h}\right)\right) \text{ and } \Psi' = i\frac{2\pi\kappa}{\Delta T}\sin\left(\frac{\pi z}{h}\right)\left(\cos\left(\frac{\pi x}{h}\right) + i\sin\left(\frac{\pi x}{h}\right)\right). \tag{3.3.3}$$

Considering the real part for physical quantities, we have

$$T' = \sin\left(\frac{\pi z}{h}\right)\cos\left(\frac{\pi x}{h}\right) \text{ and } \Psi' = -\frac{2\pi\kappa}{\Delta T}\sin\left(\frac{\pi z}{h}\right)\sin\left(\frac{\pi x}{h}\right). \tag{3.3.4}$$

We consider the combination of background temperature gradient of base state and its perturbation as

$$T = T_0 + (1 - z/h)\,\Delta T + \epsilon \sin\left(\frac{\pi z}{h}\right)\cos\left(\frac{\pi x}{h}\right), \tag{3.3.5}$$

where $\epsilon \ll 1$. The horizontal and vertical components of the velocity are provided by substituting equation (3.3.4) into equation (3.1.15) as follow

$$u' = -\frac{2\kappa}{\Delta T}\frac{\pi^2}{h}\cos\left(\frac{\pi z}{h}\right)\sin\left(\frac{\pi x}{h}\right) \text{ and } w' = \frac{2\kappa}{\Delta T}\frac{\pi^2}{h}\sin\left(\frac{\pi z}{h}\right)\cos\left(\frac{\pi x}{h}\right). \tag{3.3.6}$$

The stream-function from equation (3.3.4) is plotted in Figure 3.2 with the perturbed background temperature distribution from equation (3.3.5) as well. Figure 3.2 represents the cellular patterns that appear as the fluid experiences convection due to density difference. The flow in Figure 3.3 can be interpreted relating to how the temperature is high or low. Where there is a peak of temperature, the flow is upward, see at $x = \pm 2$ and at $x = 0$. Where there is a trough of temperature, the flow is downward see at $x = \pm 1$. Then the flow completes the circulation, as it is shown by the vector field, in the horizontal flow.

In fact, as temperature increases, hot fluid moves upward into a cooler area and gradually loses its heat. As it continues to move, it experiences the temperature difference and deviates until it becomes tangential to the top boundary. It continues to deviate in the downward motion to complete the circulation where it becomes tangential to the bottom boundary.

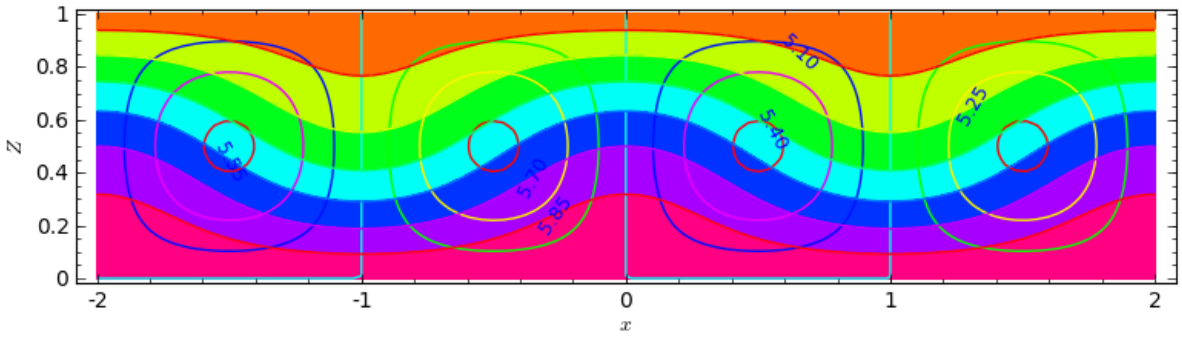

Figure 3.2: Background colour scale:The orange color at top for low and pink at the bottom for high temperature; lines are contours of Ψ', $i.e$ streamlines in the (x, z) plane for $Ra = 4\pi^2$, the value of $\epsilon = 0.2$.

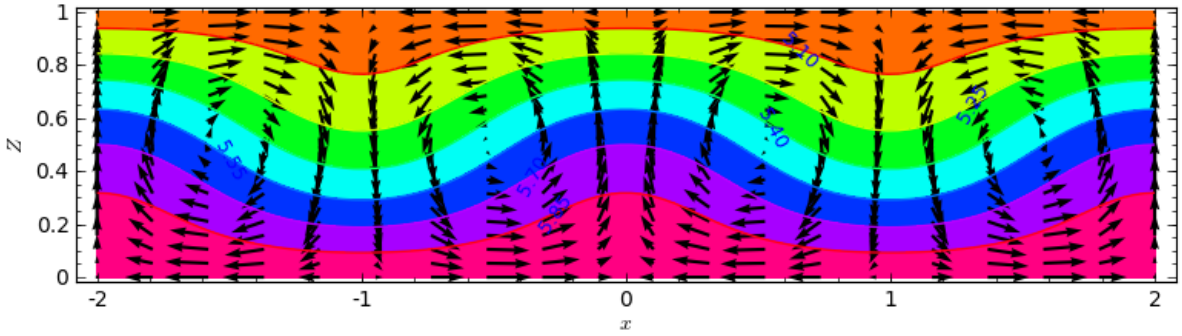

Figure 3.3: Background colour scale:The orange color at top for low and pink at the bottom for high temperature ; vectors show (u', w') in the (x, z) plane for $Ra = 4\pi^2$, the value of $\epsilon = 0.2$.

4. Double-Diffusive Convection

In this section, the double-diffusive convection that involves thermal and salinity gradients is described and analysed using linear perturbation theory. The non-linear analysis is also studied using the Galerkin approximation method. Figure 4.1 shows the system: the porous layer has height h; the thermal and salinity gradients are allowed to be negative or positive. They diffuse but at different rates.

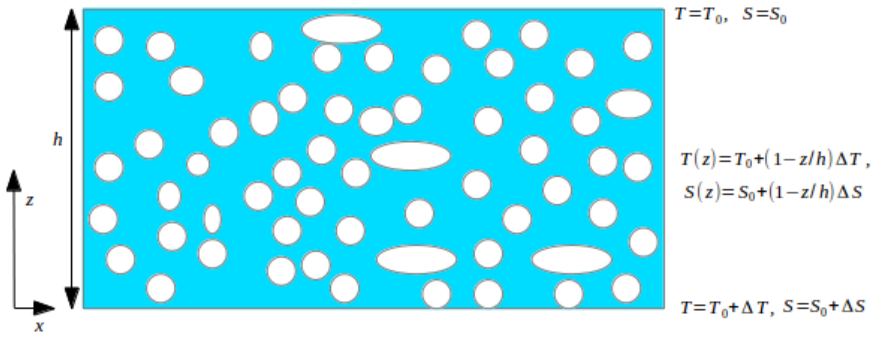

Figure 4.1: A sketch for porous layer with height h, the blue color represents water, white circles represent matrix like sandstone. Here ΔT or ΔS can be negative or positive.

4.1 Linear stability analysis

We say that the system experiences double diffusion when both heat and salt diffuse. The diffusivity of salt in liquid (say water) is small compared to that of heat (Kundu et al., 2012). We assume that the temperature gradient and salinity gradient are in the vertical direction.

The system that we are considering is the same as that in chapter 3, except that there is salt present in the fluid located in the pores. We consider the density of the fluid to depend on temperature and salinity as presented in equation (2.1.2). But now both the temperature gradient and salinity gradient may be either positive or negative.

The steady state of rest of the system is given by $u = v = w = 0$, $p = p_0(z)$, $\frac{\partial p_0}{\partial z} = -\rho g$.

The temperature depends on z as provided in equation (3.0.4), the salinity also depends on z as

$$S = S_0 + \left(1 - \frac{z}{h}\right) \Delta S, \tag{4.1.1}$$

so that at the lower boundary we have $T = T_0 + \Delta T, S = S_0 + \Delta S$, while at the upper boundary $T = T_0, S = S_0$.

4.1.1 Perturbation of the steady state of rest.

The small perturbations give the equations (3.1.1) – (3.1.3) and an addition of salinity as

$$S = S_0 + \left(1 - \frac{z}{h}\right)\Delta S + S'(x, y, z, t). \tag{4.1.2}$$

Consider equation (3.1.10), and replace the density by its equivalent from equation (2.1.2), we have

$$\frac{\partial p'}{\partial z} = -\frac{\mu}{K}w - \rho_0 g\left(1 - \alpha T + \beta S\right) - \frac{\partial p_0}{\partial z}. \tag{4.1.3}$$

After introducing the perturbations to T and S and cancelling the terms relating to $\frac{\partial p_0}{\partial z}$, we have

$$\frac{\partial p'}{\partial z} = -\frac{\mu}{K}w + \rho_0 g\alpha T' - \rho_0 g\beta S'. \tag{4.1.4}$$

Then we have the equation (3.1.10) as

$$\overrightarrow{\nabla} p' = -\frac{\mu}{K}\overrightarrow{u} + \left(\rho_0 g\alpha T' - \rho_0 g\beta S'\right)\overrightarrow{k}. \tag{4.1.5}$$

If we take the curl of this equation we obtain

$$\frac{\mu}{K}\overrightarrow{\nabla} \times \overrightarrow{u} + \overrightarrow{\nabla} \times \left(\left(\rho_0 g\alpha T' - \rho_0 g\beta S'\right)\overrightarrow{k}\right) = 0. \tag{4.1.6}$$

Let us introduce perturbations to equation (2.3.4), we have

$$\phi\frac{\partial\left(S_0 + \left(1 - \frac{z}{h}\right)\Delta S + S'\right)}{\partial t} + \overrightarrow{u}'.\overrightarrow{\nabla}\left(S_0 + \left(1 - \frac{z}{h}\right)\Delta S + S'\right) = \phi D\nabla^2\left(S_0 + \left(1 - \frac{z}{h}\right)\Delta S + S'\right). \tag{4.1.7}$$

Only S' and $\overrightarrow{u}'$ are not constant, so we have

$$\phi\frac{\partial S'}{\partial t} + \overrightarrow{u}'.\overrightarrow{\nabla}S' - \overrightarrow{u}'.\overrightarrow{\nabla}\left(\frac{z\Delta S}{h}\right) = \phi D\nabla^2 S'. \tag{4.1.8}$$

We neglect $\overrightarrow{u}'.\overrightarrow{\nabla}S'$ because it is a product of two small quantities, and write

$$\phi\frac{\partial S'}{\partial t} - \overrightarrow{u}'.\overrightarrow{\nabla}\left(\frac{z\Delta S}{h}\right) = \phi D\nabla^2 S'. \tag{4.1.9}$$

Using $\overrightarrow{u}' = (u', v', w')$ and $\overrightarrow{\nabla}\left(\frac{z\Delta S}{h}\right) = \left(0, 0, \frac{\Delta S}{h}\right)$, we write

$$\phi\frac{\partial S'}{\partial t} - w'\frac{\Delta S}{h} = \phi D\nabla^2 S'. \tag{4.1.10}$$

Introducing the streamfunction ψ' as we did in chapter 3, we get the following set of equations

$$\frac{\partial^2\psi'}{\partial x^2} + \frac{\partial^2\psi'}{\partial z^2} = \frac{K}{\mu}\rho_0 g\left(-\alpha\frac{\partial T'}{\partial x} + \beta\frac{\partial S'}{\partial x}\right), \tag{4.1.11}$$

$$M\frac{\partial T'}{\partial t} + \frac{\partial\psi'}{\partial x}\frac{\Delta T}{h} = \kappa\nabla^2 T', \tag{4.1.12}$$

$$\phi\frac{\partial S'}{\partial t}+\frac{\partial \psi'}{\partial x}\frac{\Delta S}{h}=\phi D\nabla^2 S'. \tag{4.1.13}$$

We define according to Phillips (2009), the dimensionless variables σ^*, θ^*, Ψ^*, t^*, x^* and z^* such that

$$S=\sigma^*\Delta S, T'=\theta^*\Delta T, \psi'=\frac{K}{\mu}\rho_0 gh\alpha\Delta T\Psi^*, t=\frac{h^2}{\kappa}t^* \text{ and } (x,z)=h(x^*,z^*). \tag{4.1.14}$$

Here, σ^* represents the salinity in dimensionless analysis, T^* represents the temperature, Ψ^* represents the stream function, t^* represents time and (x^*, z^*) are the horizontal and vertical coordinates respectively.

Substituting equation (4.1.14) into equation (4.1.11), we have

$$\frac{\partial^2\Psi^*}{\partial x^{*2}}+\frac{\partial^2\Psi^*}{\partial z^{*2}}=-\frac{\partial\theta}{\partial x^*}+\frac{\beta\Delta S}{\alpha\Delta T}\frac{\partial\sigma^*}{\partial x^*}. \tag{4.1.15}$$

Applying the transformations to equation (4.1.12), we have

$$M\Delta T\frac{\kappa}{h^2}\frac{\partial\theta^*}{\partial t^*}+\frac{(\Delta T)^2}{h}\frac{K}{\mu}\rho_0 g\alpha\frac{\partial\Psi^*}{\partial x^*}=\kappa\frac{\Delta T}{h^2}\nabla^2\theta^*. \tag{4.1.16}$$

Dividing equation (4.1.16) by $\kappa\frac{\Delta T}{h^2}$ and introducing kinematic viscosity $\nu=\frac{\mu}{\rho_0}$, we have

$$M\frac{\partial\theta^*}{\partial t^*}+\frac{K}{\nu\kappa}gh\alpha\Delta T\frac{\partial\Psi^*}{\partial x^*}=\nabla^2\theta^*. \tag{4.1.17}$$

This can be written as

$$M\frac{\partial\theta^*}{\partial t^*}+(Ra)\frac{\partial\Psi^*}{\partial x^*}=\nabla^2\theta^*, \tag{4.1.18}$$

where $Ra=\frac{K}{\nu\kappa}gh\alpha\Delta T$ is the Rayleigh number.

Applying again the transformations to equation (4.1.13) and dividing both sides by $\kappa\frac{\Delta S}{h^2}$, we have

$$\phi\frac{\partial\sigma^*}{\partial t^*}+(Ra)\frac{\partial\Psi^*}{\partial x^*}=\phi Le\nabla^2\sigma^*, \tag{4.1.19}$$

where for fixed temperature and salinity, at $z^*=0$ and at $z^*=1$, $\theta^*=\sigma^*=0, \Psi^*=0$. $Le=\frac{D}{\kappa}$ is called the Lewis number, which is typically small and of order of 10^{-2} but we can take $Le=O(10^{-1})$ for plotting purposes.

Proceeding as in chapter 3, the solutions of equations (4.1.15), (4.1.18) and (4.1.19) have the form

$$\theta^*=A_1\sin(m^*\pi z^*)e^{ik^*\pi x^*}e^{nt^*}, \tag{4.1.20}$$

$$\Psi^*=B_1\sin(m^*\pi z^*)e^{ik^*\pi x^*}e^{nt^*}, \tag{4.1.21}$$

and

$$\sigma^*=C_1\sin(m^*\pi z^*)e^{ik^*\pi x^*}e^{nt^*}, \tag{4.1.22}$$

where A_1, B_1 and C_1 are real constants. Replacing these solutions in (4.1.15), (4.1.18) and (4.1.19), and after simplification we get

$$ik^*\pi A_1 - ik^*\pi\frac{\beta\Delta S}{\alpha\Delta T}C_1 - \pi^2\left(k^{*2}+m^{*2}\right)B_1 = 0, \tag{4.1.23}$$

$$\left(Mn + \pi^2\left(k^{*2}+m^{*2}\right)\right)A_1 + i(Ra)k^*\pi B_1 = 0, \tag{4.1.24}$$

$$\left(\phi n + \phi Le\pi^2\left(k^{*2}+m^{*2}\right)\right)C_1 + i(Ra)k^*\pi B_1 = 0. \tag{4.1.25}$$

Solving simultaneously the system from equations (4.1.23), (4.1.24) and (4.1.25), we require that the determinant vanish,

$$\begin{vmatrix} ik^*\pi & -ik^*\pi\frac{\beta\Delta S}{\alpha\Delta T} & -\pi^2\left(k^{*2}+m^{*2}\right) \\ Mn+\pi^2\left(k^{*2}+m^{*2}\right) & 0 & i(Ra)k^*\pi \\ 0 & \phi n+\phi Le\pi^2\left(k^{*2}+m^{*2}\right) & i(Ra)k^*\pi \end{vmatrix} = 0.$$

The determinant expansion gives

$$\begin{aligned} &k^{*2}\pi^2(Ra)\phi\left(n+Le\left(k^{*2}+m^{*2}\right)\right) - k^{*2}\pi^2(Ra)\frac{\beta\Delta S}{\alpha\Delta T}\left(Mn+\pi^2\left(k^{*2}+m^{*2}\right)\right) \\ &-\pi^2\left(k^{*2}+m^{*2}\right)\left(Mn+\pi^2\left(k^{*2}+m^{*2}\right)\right)\left(\phi n+\phi\pi^2 Le\left(k^{*2}+m^{*2}\right)\right) = 0. \end{aligned}$$

Expanding the product we have

$$\begin{aligned} &k^{*2}\pi^2\phi(Ra)n + Lek^{*2}\pi^4\phi(Ra)\left(k^{*2}+m^{*2}\right) - k^{*2}\pi^2(Ra)\frac{\beta\Delta S}{\alpha\Delta T}Mn - k^{*2}\pi^4(Ra)\frac{\beta\Delta S}{\alpha\Delta T}\left(k^{*2}+m^{*2}\right) \\ &-\pi^2\left(k^{*2}+m^{*2}\right)M\phi n^2 - \pi^4\left(k^{*2}+m^{*2}\right)^2\phi n - \pi^6\left(k^{*2}+m^{*2}\right)^3\phi Le - \pi^4\left(k^{*2}+m^{*2}\right)^2\phi LeMn = 0 \end{aligned}$$

Dividing by $-\phi\pi^2\left(k^{*2}+m^{*2}\right)$ and grouping the terms together, we have

$$\begin{aligned} Mn^2 + \left(\frac{k^{*2}(Ra)}{\left(k^{*2}+m^{*2}\right)}\left(-1+\frac{\beta\Delta S}{\alpha\Delta T}\frac{M}{\phi}\right) + \pi^2\left(k^{*2}+m^{*2}\right) + \pi^2\left(k^{*2}+m^{*2}\right)LeM\right)n \\ -Lek^{*2}\pi^2(Ra) + k^{*2}\pi^2(Ra)\frac{\beta\Delta S}{\alpha\Delta T}\frac{1}{\phi} + \pi^4\left(k^{*2}+m^{*2}\right)^2 Le = 0. \end{aligned} \tag{4.1.26}$$

Equation (4.1.1) can be written in the form of quadratic equation in n as

$$an^2 + bn + c = 0, \tag{4.1.27}$$

where

$$a = M, \tag{4.1.28}$$

$$b = \frac{k^{*2}(Ra)}{\left(k^{*2}+m^{*2}\right)}\left(-1+\frac{\beta\Delta S}{\alpha\Delta T}\frac{M}{\phi}\right) + \pi^2\left(k^{*2}+m^{*2}\right) + \pi^2\left(k^{*2}+m^{*2}\right)LeM \tag{4.1.29}$$

and

$$c = -Lek^{*2}\pi^2(Ra) + k^{*2}\pi^2(Ra)\frac{\beta\Delta S}{\alpha\Delta T}\frac{1}{\phi} + \pi^4\left(k^{*2}+m^{*2}\right)^2 Le. \tag{4.1.30}$$

4.1.2 Double-diffusive stability analysis.

From the equation (4.1.27), let us define

$$Ra_s = (Ra)\frac{\beta\Delta S}{\alpha\Delta T} \tag{4.1.31}$$

so that

$$b = -\frac{k^{*2}(Ra)}{(k^{*2}+m^{*2})} + \frac{k^{*2}Ra_s}{(k^{*2}+m^{*2})}\frac{M}{\phi} + \pi^2\left(k^{*2}+m^{*2}\right)(1+LeM) \tag{4.1.32}$$

and

$$c = -Lek^{*2}\pi^2(Ra) + \frac{k^{*2}\pi^2}{\phi}Ra_s + \pi^4\left(k^{*2}+m^{*2}\right)^2 Le. \tag{4.1.33}$$

The quadratic equation (4.1.27) has the solutions n_+ and n_- as

$$n_\pm = \frac{-b \pm \sqrt{b^2-4ac}}{2a} \tag{4.1.34}$$

We must consider two cases for transition to instability. The first case is when $b^2-4ac>0$, we have n_+ and n_- as purely real.

But $n_- < n_+$, so when $n_+ < 0$ for all k^*, m^* the base state is stable, while if $n_+ > 0$ for some k^* and m^*, the base state is unstable.

The stability boundaries that separate stable regions from unstable one is at $n_+ = 0$,

$$\frac{-b+\sqrt{b^2-4ac}}{2a} = 0 \Longleftrightarrow b = \sqrt{b^2-4ac} \Longleftrightarrow 4ac = 0 \Longleftrightarrow c = 0\,(\text{ since } 4a>0)\,. \tag{4.1.35}$$

The condition $c=0$ means that

$$-Le\phi k^{*2}\pi^2(Ra) + \frac{k^{*2}\pi^2}{\phi}Ra_s = -\pi^4\left(k^{*2}+m^{*2}\right)^2 Le. \tag{4.1.36}$$

Then we have the line defined by

$$L_1 \equiv Ra = \frac{1}{\phi Le}Ra_s + \frac{\pi^2\left(k^{*2}+m^{*2}\right)^2}{k^{*2}}. \tag{4.1.37}$$

The intersection of line L_1 with the Ra_s-axis is at the point

$$(Ra_{s0}, 0) = \left(-\frac{\pi^2\left(k^{*2}+m^{*2}\right)Le\phi}{k^{*2}}, 0\right). \tag{4.1.38}$$

The intersection of line L_1 with the $Ra-$axis is at the point

$$(0, Ra_0) = \left(0, \frac{\pi^2\left(k^{*2}+m^{*2}\right)}{k^{*2}}\right). \tag{4.1.39}$$

The second case is when $b^2 - 4ac \leq 0$, n_+ and n_- are complex numbers. We write

$$n_\pm = \frac{-b \pm i\sqrt{4ac - b^2}}{2a}. \tag{4.1.40}$$

Here the real parts for n_+ and for n_- are equal to

$$\mathrm{Re}(n_+) = \mathrm{Re}(n_-) = -\frac{b}{2a}. \tag{4.1.41}$$

If $b > 0$, then $\mathrm{Re}(n_+) < 0$ since $a > 0$, so the base state is stable to this perturbation. If $b < 0$, then the base state is unstable to this perturbation.

Then the boundary of the stable region is at $\mathrm{Re}(n_+) = 0$, which means that

$$-\frac{b}{2a} = 0 \Longrightarrow b = 0. \tag{4.1.42}$$

Using the condition $b = 0$, we have

$$-\frac{k^{*2}(Ra)}{(k^{*2} + m^{*2})} + \frac{k^{*2} Ra_s}{(k^{*2} + m^{*2})}\frac{M}{\phi} = -\pi^2\left(k^{*2} + m^{*2}\right)(1 + LeM). \tag{4.1.43}$$

Then we have the line defined by

$$L_2 \equiv Ra = \frac{M}{\phi} Ra_s + \frac{\pi^2\left(k^{*2} + m^{*2}\right)^2}{k^{*2}}(1 + LeM). \tag{4.1.44}$$

The intersection of line L_2 with the Ra_s-axis is at the point

$$(Ra_{s0}, 0) = \left(-\frac{\pi^2\left(k^{*2} + m^{*2}\right)}{k^{*2}}\frac{\phi}{M}(1 + LeM), 0\right). \tag{4.1.45}$$

The intersection of line L_2 with the $Ra-$axis is at the point

$$(0, Ra_0) = \left(0, \frac{\pi^2\left(k^{*2} + m^{*2}\right)}{k^{*2}}(1 + LeM)\right). \tag{4.1.46}$$

We have to minimize the line L_1 and L_2 over k^* and m^* to obtain the minimum value for Ra. Let us differentiate L_1 with respect to k^*.

$$\frac{\partial L_1}{\partial k^*} = \pi^2\left(2k^* - \frac{2m^{*4}}{k^{*3}}\right) = 0. \tag{4.1.47}$$

This gives

$$k^{*4} = m^{*4} \text{ which implies that } k^* = m^*. \tag{4.1.48}$$

We differentiate L_2 with respect to k^* to obtain the same relation between k^* and m^*.

Since m^* is an integer and $m^* \neq 0$ for non-trivial solutions, the lowest value that it can take is $m^* = 1$. This implies that $k^* = 1$ from the minimization condition.

At this stage the line equations L_1 and L_2 have the minimized expressions

$$L_{1min} \equiv Ra^1_{min} = \frac{Ra_s}{\phi Le} + 4\pi^2, \tag{4.1.49}$$

and

$$L_{2min} \equiv Ra^2_{min} = \frac{MRa_s}{\phi} + 4\pi^2\left(1 + LeM\right). \tag{4.1.50}$$

4.1.3 Solutions for marginally stable modes.

We want to plot the temperature function and the flow field in the (x, z) plane. Therefore we need to find out the coefficients A_1, B_1 and C_1 of equations (4.1.20), (4.1.21) and (4.1.22). Since the roots $n_\pm = n_r \pm in_i$, firstly we consider where the minimized values $k^* = m^* = 1$ are for $n_r = n_i = 0$ and we can work in unit such that $A_1 = 1$. Substituting this value of A_1 in the equation (4.1.24), we get the expression for B_1 to be

$$B_1 = \frac{2\pi}{Ra^1_{min}} i. \tag{4.1.51}$$

Substituting this value of B_1 into equation (4.1.25), we get the expression for C_1 to be

$$C_1 = \frac{1}{\phi Le}. \tag{4.1.52}$$

Hence the equations (4.1.20), (4.1.21) and (4.1.22) will be

$$\theta^* = \sin(\pi z^*)\left(\cos(\pi x^*) + i\sin(\pi x^*)\right), \tag{4.1.53}$$

$$\Psi^* = i\frac{2\pi}{Ra^1_{min}}\sin(\pi z^*)\left(\cos(\pi x^*) + i\sin(\pi x^*)\right), \tag{4.1.54}$$

and

$$\sigma^* = \frac{1}{\phi Le}\sin(\pi z^*)\left(\cos(\pi x^*) + i\sin(\pi x^*)\right). \tag{4.1.55}$$

By considering the real parts for physical quantities, we have

$$\theta^* = \sin(\pi z^*)\cos(\pi x^*), \tag{4.1.56}$$

$$\Psi^* = -\frac{2\pi}{Ra^1_{min}}\sin(\pi z^*)\sin(\pi x^*), \tag{4.1.57}$$

and

$$\sigma^* = \frac{1}{\phi Le}\sin(\pi z^*)\cos(\pi x^*). \tag{4.1.58}$$

We have a line L_1 that gives the minimized value of Ra^1_{min}. Substituting this minimum value of Ra_{min} into equation (4.1.49), we obtain the streamfunction Ψ^* as

$$\Psi^* = -\frac{2\pi}{\left(\frac{Ra_s}{\phi Le} + 4\pi^2\right)}\sin(\pi z^*)\sin(\pi x^*). \tag{4.1.59}$$

The horizontal and vertical velocity components are

$$u' = -\frac{2\pi^2}{\left(\frac{Ra_s}{\phi Le} + 4\pi^2\right)} \cos(\pi z^*) \sin(\pi x^*), \tag{4.1.60}$$

$$w' = \frac{2\pi^2}{\left(\frac{Ra_s}{\phi Le} + 4\pi^2\right)} \sin(\pi z^*) \cos(\pi x^*). \tag{4.1.61}$$

Secondly, we are considering real part of n to be zero and the imaginary part to be different from zero, where the minimized values $k^* = m^* = 1$ are for $n_r = 0$ but $n_i \neq 0$. We use these conditions to find the coefficients A_1, B_1 and C_1. Again we can work in units such that $A_1 = 1$. Then

$$n_i = \frac{\sqrt{|4ac - b^2|}}{2a}, \tag{4.1.62}$$

where the minimized values for a, b and c are

$$a = M,\ b = -\frac{Ra}{2} + \frac{Ra_s M}{2\phi} + 2\pi^2(1 + LeM) \text{ and } c = -Le\pi^2 Ra + \pi^2 \frac{Ra_s}{\phi} + 4\pi^4 Le \tag{4.1.63}$$

respectively.

Now we substitute the value of A_1 in the equation (4.1.24) to find B_1. So we have

$$iMn_i + 2\pi_i^2 Ra\pi B_1 = 0. \tag{4.1.64}$$

This is

$$B_1 = -\frac{Mn_i}{Ra\pi} + i\frac{2\pi}{Ra}. \tag{4.1.65}$$

Substituting this value of B_1 in the equation (4.1.25) to find the coefficient C_1, we get

$$(in_i + 2Le\pi^2)\phi C_1 + iRa\pi(-\frac{Mn_i}{Ra\pi} + i\frac{2\pi}{Ra}) = 0. \tag{4.1.66}$$

This is

$$C_1 = \frac{iMn_i + 2\pi}{(in_i + 2Le\pi^2)\phi}. \tag{4.1.67}$$

By conjugating the complex number in the denominator, we have

$$C_1 = \frac{(iMn_i + 2\pi)}{(in_i + 2Le\pi^2)\phi} \frac{(-in_i + 2Le\pi^2)}{(-in_i + 2Le\pi^2)}. \tag{4.1.68}$$

Then we have

$$C_1 = \frac{Mn_i^2 + 4Le\pi^4}{(n_i^2 + (2Le\pi^2)^2)\phi} + i\frac{2Mn_i Le\pi^2 - 2\pi^2 n_i}{(n_i^2 + (2Le\pi^2)^2)\phi}. \tag{4.1.69}$$

Substituting these values of A_1, B_1 and C_1 in the set of equations (4.1.20) – (4.1.22), we have the temperature as

$$\theta^* = \sin(\pi z^*) \exp(i\pi x^*). \exp(nt^*). \tag{4.1.70}$$

Since $n = \pm n_i$, we have

$$\theta^* = \sin(\pi z^*)\exp(i\pi x^*)\left(\exp(in_i t^*) + \exp(-in_i t^*)\right). \tag{4.1.71}$$

This is

$$\theta^* = 2\sin(\pi z^*)\left(\cos(\pi x^*) + i\sin(\pi x^*)\right)\cos(n_i t). \tag{4.1.72}$$

We consider the real part of this function to obtain the physical quantity. The we have

$$\theta^* = 2\sin(\pi z^*)\cos(\pi x^*)\cos(n_i t). \tag{4.1.73}$$

Then the streamfunction Ψ^* will become

$$\Psi^* = B_1^0 \sin(\pi z^*)\exp(i\pi x^*)\exp(in_i t^*) + B_1^1 \sin(\pi z^*)\exp(i\pi x^*)\exp(-in_i t^*), \tag{4.1.74}$$

where B_1^0 and B_1^1 are the constants. Replacing the expressions of these coefficients B_1^0 and B_1^1, we have

$$\Psi^* = \left(-\frac{Mn_i}{Ra\pi} + i\frac{2\pi}{Ra}\right)\sin(\pi z^*)\left(\cos(\pi x^*) + i\sin(\pi x^*)\right)\left(\cos(n_i t^*) + i\sin(n_i t^*)\right)$$
$$+ \left(\frac{Mn_i}{Ra\pi} + i\frac{2\pi}{Ra}\right)\sin(\pi z^*)\left(\cos(\pi x^*) + i\sin(\pi x^*)\right)\left(\cos(n_i t^*) - i\sin(n_i t^*)\right). \tag{4.1.75}$$

Expanding and collecting like terms we have

$$\Psi^* = i\frac{4\pi}{Ra}\sin(\pi z^*)\cos(\pi x^*)\cos(n_i t^*) - i\frac{2Mn_i}{Ra\pi}\sin(\pi z^*)\cos(\pi x^*)\sin(n_i t^*)$$
$$- \frac{4\pi}{Ra}\sin(\pi z^*)\sin(\pi x^*)\cos(n_i t^*) + \frac{2Mn_i}{Ra\pi}\sin(\pi z^*)\sin(\pi x^*)\sin(n_i t^*). \tag{4.1.76}$$

Taking the real part for the physical quantity, we have

$$\Psi^* = -\frac{4\pi}{Ra}\sin(\pi z^*)\sin(\pi x^*)\cos(n_i t^*) + \frac{2Mn_i}{Ra\pi}\sin(\pi z^*)\sin(\pi x^*)\sin(n_i t^*). \tag{4.1.77}$$

The horizontal and vertical vector components u' and w' are

$$u' = -\frac{4\pi^2}{Ra}\cos(\pi z^*)\sin(\pi x^*)\cos(n_i t^*) + \frac{2Mn_i}{Ra\pi}\sin(\pi z^*)\sin(\pi x^*)\sin(n_i t^*), \tag{4.1.78}$$

$$w' = \frac{4\pi^2}{Ra}\sin(\pi z^*)\cos(\pi x^*)\cos(n_i t^*) + \frac{2Mn_i}{Ra\pi}\sin(\pi z^*)\sin(\pi x^*)\sin(n_i t^*). \tag{4.1.79}$$

The concentration will be

$$\sigma^* = \left(\frac{Mn_i^2 + 4Le\pi^4}{(n_i^2 + (2Le\pi^2)^2)\phi} + i\frac{2Mn_i Le\pi^2 - 2\pi^2 n_i}{(n_i^2 + (2Le\pi^2)^2)\phi}\right)\sin(\pi z^*)\times$$
$$\left(\cos(\pi x^*) + i\sin(\pi x^*)\right)\left(\cos(n_i t^*) + i\sin(n_i t^*)\right)$$
$$+ \left(\frac{Mn_i^2 + 4Le\pi^4}{(n_i^2 + (2Le\pi^2)^2)\phi} - i\frac{2Mn_i Le\pi^2 - 2\pi^2 n_i}{(n_i^2 + (2Le\pi^2)^2)\phi}\right)\sin(\pi z^*)\times \tag{4.1.80}$$
$$\left(\cos(\pi x^*) + i\sin(\pi x^*)\right)\left(\cos(n_i t^*) - i\sin(n_i t^*)\right).$$

Also expanding and collecting like terms we have,

$$\sigma^* = \frac{2Mn_i^2 + 4Le\pi^4}{(n_i^2 + (2Le\pi^2)^2)\phi} \sin(\pi z^*)\cos(\pi x^*)\cos(n_i t^*) - \frac{2Mn_iLe\pi^2 - 2\pi^2 n_i}{(n_i^2 + (2Le\pi^2)^2)\phi} \sin(\pi z^*)\cos(\pi x^*)\sin(n_i t^*)$$
$$+ i\frac{2Mn_iLe\pi^2 - 2\pi^2 n_i}{(n_i^2 + (2Le\pi^2)^2)\phi} \sin(\pi z^*)\sin(\pi x^*)\cos(n_i t^*) - i\frac{2Mn_iLe\pi^2 - 2\pi^2 n_i}{(n_i^2 + (2Le\pi^2)^2)\phi} \sin(\pi z^*)\sin(\pi x^*)\sin(n_i t^*). \tag{4.1.81}$$

Taking the real part for the physical quantity, we have

$$\sigma^* = \left(\frac{2Mn_i^2 + 4Le\pi^4}{(n_i^2 + (2Le\pi^2)^2)\phi} \cos(n_i t^*) - \frac{2Mn_iLe\pi^2 - 2\pi^2 n_i}{(n_i^2 + (2Le\pi^2)^2)\phi} \sin(n_i t^*) \right) \sin(\pi z^*)\cos(\pi x^*). \tag{4.1.82}$$

4.1.4 Linear stability results.

The stability diagram for double-diffusive convection drawn in Figure 4.2 describes the situation where the fluid can be stable or unstable. This figure contains four quadrants. We will use equations (2.1.2), (3.0.4) and (4.1.1) to locate the temperature salinity of water within the saturated porous layer. In the first quadrant $Ra_s > 0$, which says that salinity gradient is negative, while Ra is positive, means that the thermal gradient is negative. This says that cold fresh water overlies the hot salty water. The second quadrant has negative thermal gradient and positive salinity. Here cold salty water overlies the hot fresh water. The third quadrant has positive thermal and salt gradients. This means that hot salty water overlies cold fresh water. The last quadrant has positive thermal gradient and negative salinity gradient. Here hot fresh water overlies cold salty water.

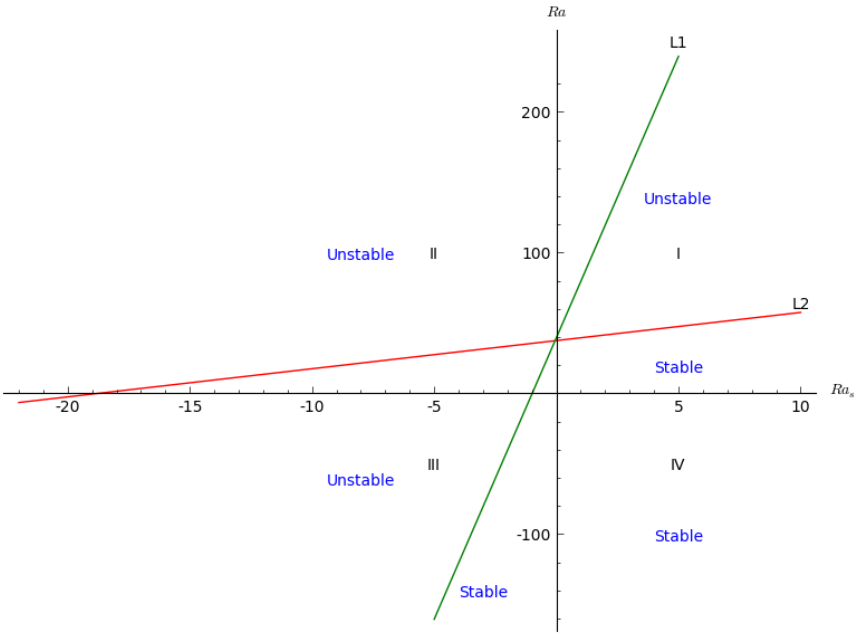

Figure 4.2: Stability diagram for double-diffusive convection in (Ra_s, Ra) plane

We have to consider the stability boundaries on which $\mathrm{Re}(n_+) = 0$, where n_+ is defined by the equation (4.1.40). This boundary consists of two lines. We have the red line L_2 which is from

the root n_+ of the quadratic equation when its imaginary part is not zero. The line L_1 in green represents the root n_+ when it is purely real.

Any point below L_1 and L_2 is in the stable region. Any other point in the (Ra_s, Ra) plane is in the unstable region as indicated in Figure 4.2. Points belonging to the right hand part of line L_2 are neutrally stable (also called 'marginal state'), as are the points belonging to the left hand part of L_1.

When the state of the system is passing from the stable region to the unstable region, two crucial things may happen. The first one is when the system is passing from the stable region to the unstable region through line L_1, where the root n_+ is real, the perturbation starts to grow exponentially; this is called direct onset. We can have this situation in the third quadrant where hot, salty water overlies the cold fresh water. Consider a hot, salty fluid element which is displaced downward. Since the temperature diffuses faster, it will lose temperature but it will remain with its salt concentration. Then it will be more dense than its surroundings and will continue to descend. Since the surrounding is viscous fluid, the viscosity will tend to stop the flow and it is called a stabilising effect however, when the salinity forces the flow, is called a destabilising effect. Phillips (2009) discussed that when a small region of a fluid is moved upward, it becomes hotter compared to its surrounding although it remains fresh. It will therefore possess less density which will allow it to continue the upward motion. This kind of motion produces the effect called fingering which was discussed by Turner (1973).

The second way for instability to develop is that at the onset, the flow is oscillatory. This is observed when the state of the system is passing from stable region to unstable region through line L_2. This is happening in the first quadrant where cold fresh water overlies hot salty water. In this case the growth rate n_+, is complex and can be represented as $n_+ = n_r + in_i$, where n_r is the real part and n_i is the imaginary part. The real part contributes to the growth or decay of the oscillation depending on whether we are in the unstable or the stable region. The imaginary part contributes to the oscillation. When the system is passing through line L_2, we will say that it is oscillatory onset. The fluid element becomes hot, it will be displaced upward and it will lose its temperature little by little but its salt concentration will remain the same. Hence it will be heavier than the surroundings. Eventually, it will tend to move back due to buoyancy, it will then oscillate.

The two Figures 4.3 and 4.4 illustrate the flow pattern at the onset of the convection. The flow is in the third quadrant, hot salty water overlies the cold fresh water. In Figure 4.4 at a point $x = \pm 1$, the flow is upward: this is where the contour is perturbed upward, so the perturbation raises water of low salinity, and thus the salinity is perturbed downward. At a point $x = \pm 2$ and at $x = 0$, the flow is downward: this is where the contour has moved downward. The fluid is heavy and flow is reinforcing the perturbation of the concentration.

In Figure 4.3, the temperature perturbations are small compared to that of concentrations. This is because the temperature diffuses faster than salt. The heat is at the top, the fluid element will move downward. It will carry hot fluid into the cold area.

We are considering the oscillatory flow over a period of 2π. We are interested in how the perturbation of temperature and that of salinity contribute to the flow over a period. The Figures 4.5 up to 4.8 (and in the Appendix, Figure A.1 to Figure A.6) are showing the sequence

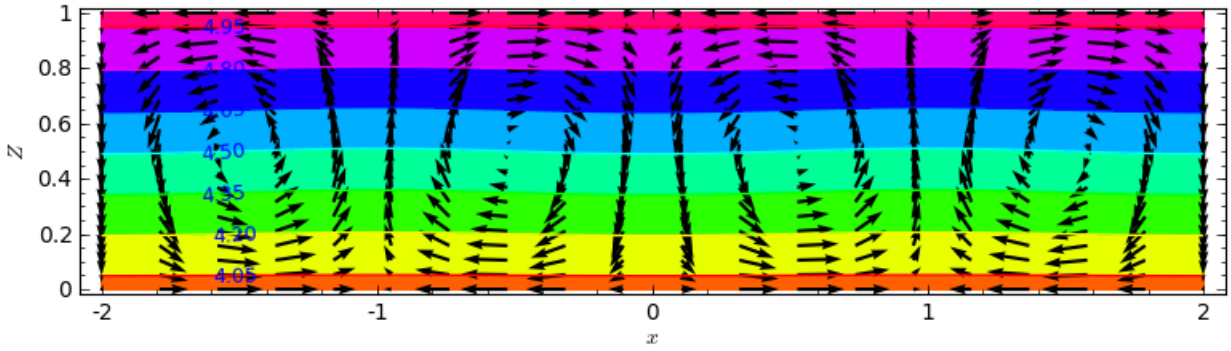

Figure 4.3: From third quadrant, the pink color at the top for high and orange at the bottom for low temperature and velocity field for $\epsilon = 0.01$, $Ra_s = -5$, $Ra = -160.521$, $\phi = 0.25$, $Le = 0.1$ and $M = 0.5$.

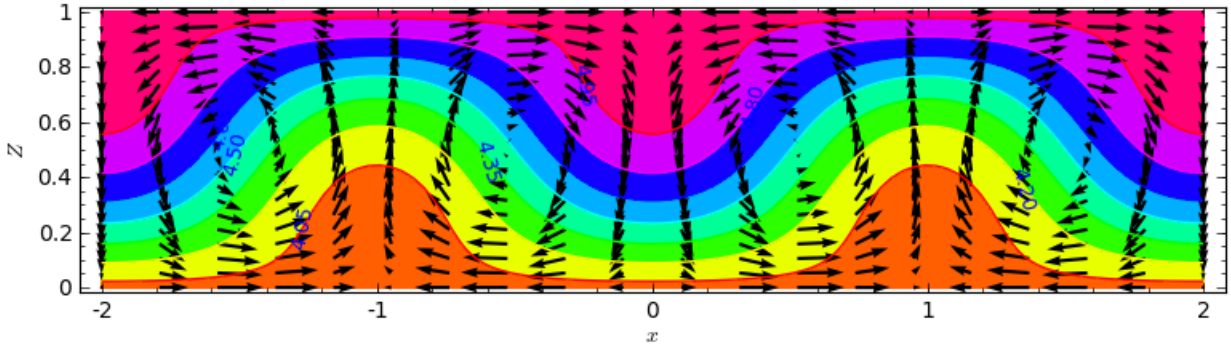

Figure 4.4: From third quadrant, the pink color at the top for high and orange at bottom for low concentration and velocity field,for $\epsilon = 0.01$, $Ra_s = -5$, $Ra = -160.521$, $\phi = 0.25$, $Le = 0.1$ and $M = 0.5$.

of the snapshots through a half period from 0 to π.

At $x = 0$, by observing Figure 4.5, the contours of temperature are perturbed upward, so the fluid is relatively hot. The contours of salinity are perturbed upward (see Figure 4.6), and the fluid is relatively salty. This means that there is competition between temperature and salt concentration. The temperature wins slightly and the flow is in the upwards direction with small magnitude.

In Figure 4.7 at $x = 0$, the temperature perturbation is smaller than the temperature in Figure 4.5 and Figure 4.6. Hence the concentration wins so that we have the flow in downwards motion with quite high magnitude (see Figure 4.8).

In Figure A.1 (see Appendix) and Figure A.2 (see Appendix) respectively at $x = 0$, it is hard to see due to the figure size but temperature and salinity perturbations are downwards. The fluid is cold and slightly salty, so it will continue downward motion, with velocity magnitude of the same order as in the previous situation presented in Figures 4.7 to 4.8.

In Figure A.3 (see Appendix) and in Figure A.4 (see Appendix) at $x = 0$, it is clear that temperature and salinity are perturbed downward respectively. But the fluid is relatively cold and

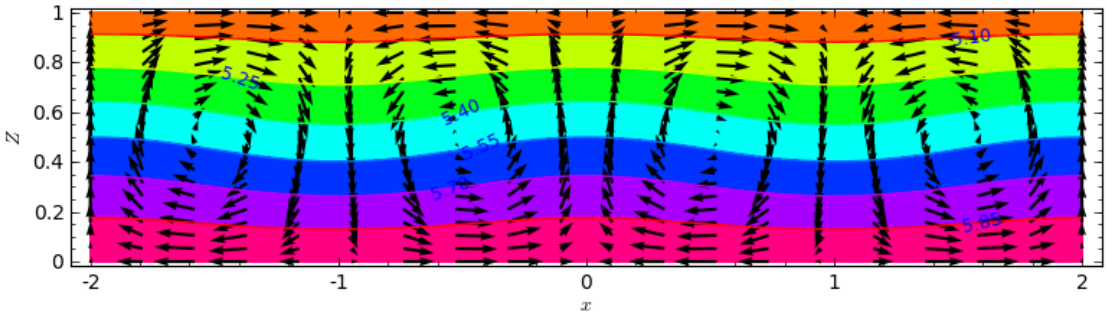

Figure 4.5: From first quadrant, the orange color at the top for low and pink at the bottom for high temperature and velocity field for $\epsilon = 0.025$, $Ra_s = 5$, $Ra = 51.542$, $\phi = 0.25$, $Le = 0.1$ and $M = 0.5$; at $n_i t^* = 0$, for $x = 0$, maximum scaled velocity $\simeq 0.767$ at $z = 0.5$.

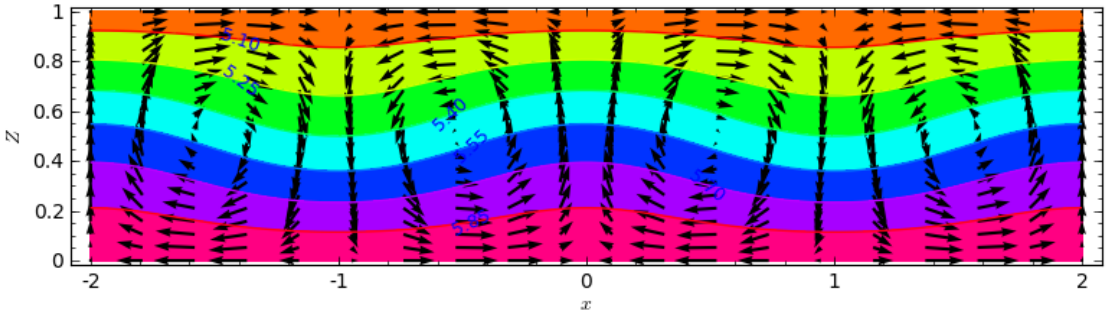

Figure 4.6: From first quadrant, the orange at the top for low and pink at the bottom for high concentration and velocity field,for $\epsilon = 0.025$, $Ra_s = 5$, $Ra = 51.542$, $\phi = 0.25$, $Le = 0.1$ and $M = 0.5$; at $n_i t^* = 0$, for $x = 0$, maximum scaled velocity $\simeq 0.767$ at $z = 0.5$.

relatively fresh. However, the coldness wins and the flow is downward, though not as strongly as it was for the situation presented in Figures $A.1$ to $A.2$ (see Appendix).

In Figure $A.5$ (see Appendix) and Figure $A.6$ (see Appendix) at $x = 0$, the situation is exactly opposite to the situation presented in Figures 4.5 to 4.6. This is the end of the downward phase and the beginning of the upward phase.

This process of upward flow motion, will be in the reverse compare to former cases until it will reach 2π to begin the next period (see AppendixA from Figure $A.7$ to Figure $A.14$). Hence the oscillations will continue as time grows.

This kind of oscillatory motion may undergo decay or growth depending on whether $\mathrm{Re}(n_\pm) \neq 0$. This will result in instability when $\mathrm{Re}(n_\pm) > 0$ and stability when $\mathrm{Re}(n_\pm) < 0$.

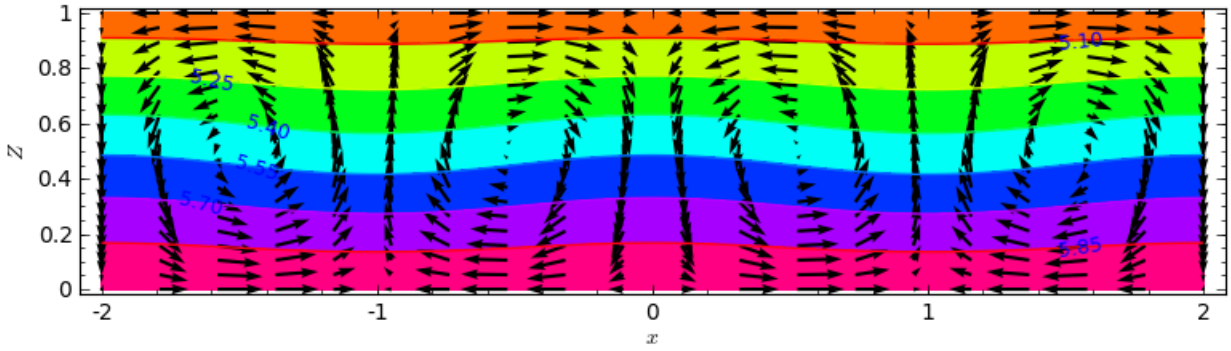

Figure 4.7: From first quadrant, the orange color at the top for low and red at the bottom for high temperature and velocity field for $\epsilon = 0.025$, $Ra_s = 5$, $Ra = 51.542$, $\phi = 0.25$, $Le = 0.1$ and $M = 0.5$; at $n_i t^* = \pi/4$ for $x = 0$, maximum scaled velocity $\simeq -5.351$ at $z = 0.5$.

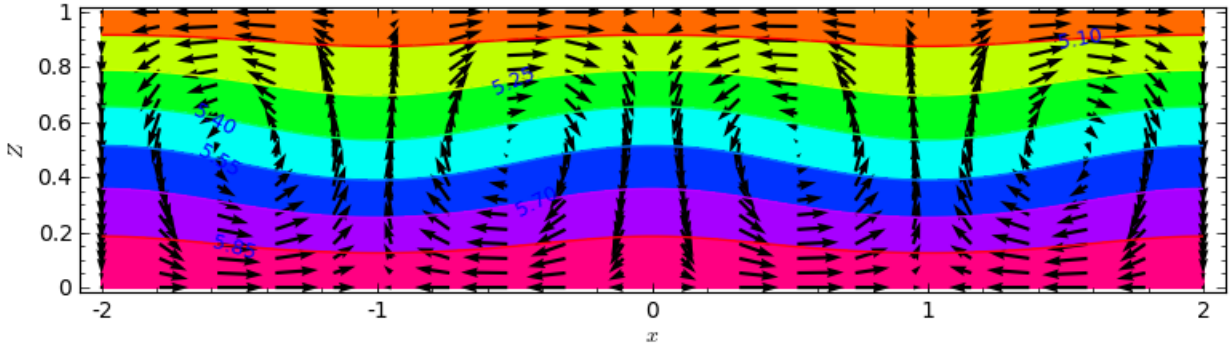

Figure 4.8: From first quadrant the orange color at the top for low and pink at the bottom for high concentration and velocity field, for $\epsilon = 0.025$, $Ra_s = 5$, $Ra = 51.542$, $\phi = 0.25$, $Le = 0.1$ and $M = 0.5$; at $n_i t^* = \pi/4$ for $x = 0$, maximum scaled velocity $\simeq -5.351$ at $z = 0.5$.

4.2 Galerkin method for non-linear double-diffusive stability analysis

When we were doing mathematical manipulation to have the partial differential equations with linear terms, we neglected the terms that should make the equations non-linear. The reason to consider these non-linear terms is because the linear analysis only predicts the infinitesimal amplitudes of perturbations but it can not predict the absolute amplitudes. In practice, when the base state is unstable, the perturbations do not grow exponentially forever, they saturate at finite amplitude. The issue is to predict this amplitude. To tackle this kind of problem, we use the Galerkin approximation method. At this stage we are now considering the governing equations of our system including the non-linear terms.

We consider the equations (3.1.13),(4.1.6) and (4.1.8) which we write in terms of dimensionless variables as

$$\frac{\partial^2 \Psi^*}{\partial x^{*2}} + \frac{\partial^2 \Psi^*}{\partial z^{*2}} + \frac{\partial \theta^*}{\partial x^*} - \frac{\beta \Delta S}{\alpha \Delta T} \frac{\partial \sigma^*}{\partial x^*} = 0, \tag{4.2.1}$$

$$M\frac{\partial\theta^*}{\partial t^*}+Ra\left(\frac{\partial\Psi^*}{\partial z^*}\frac{\partial\theta^*}{\partial x^*}-\frac{\partial\Psi^*}{\partial x^*}\frac{\partial\theta^*}{\partial z^*}\right)+Ra\frac{\partial\Psi^*}{\partial x^*}-\frac{\partial^2\theta^*}{\partial x^{*2}}-\frac{\partial^2\theta^*}{\partial z^{*2}}=0, \tag{4.2.2}$$

and

$$\frac{\partial\sigma^*}{\partial t^*}+\frac{Ra}{\phi}\left(\frac{\partial\Psi^*}{\partial z^*}\frac{\partial\sigma^*}{\partial x^*}-\frac{\partial\Psi^*}{\partial x^*}\frac{\partial\sigma^*}{\partial z^*}\right)+\frac{Ra}{\phi}\frac{\partial\Psi^*}{\partial x^*}-Le\frac{\partial^2\sigma^*}{\partial x^{*2}}-Le\frac{\partial^2\sigma^*}{\partial z^{*2}}=0. \tag{4.2.3}$$

We can deduce approximate solutions following Mamou and Vasseur (1999) and Pritchard and Richardson (2007) where they have assumed that basic circulation is as it was in the linear perturbation theory but has a time dependent coefficient. For temperature and concentration they have additional terms which are in function of the vertical axis z and time t.

We consider equations (4.2.1), (4.2.2) and (4.2.3) and use the solutions of the linear equations discussed in section 4.1, but instead of considering the exponential forms, they will be sinusoidal in x and in z. Then their coefficients are time dependent and they are not allowed to be complex.

From the linear solutions, when $k^*=m^*=1$ we have

$$\theta^*=A_1(t)\cos(\pi x^*)\sin(\pi z^*), \tag{4.2.4}$$

$$\Psi^*=B_1(t)\sin(\pi x^*)\sin(\pi z^*), \tag{4.2.5}$$

and

$$\sigma^*=C_1(t)\cos(\pi x^*)\sin(\pi z^*). \tag{4.2.6}$$

The Galerkin approximation allows us to extend these solutions to experience the weak-non linear effects. In our case, the weak non-linear effects are close to the stability boundary, the perturbations are small but not infinitesimal. When considering the solutions in equations (4.2.4) to (4.2.6) that contain the time dependent coefficients, the non-linear terms in equations (4.2.1) to (4.2.3) produce the terms proportional to $\sin(2\pi z^*)$. From this fact we extend the set of solutions (4.2.4), (4.2.5) and (4.2.6) to be

$$\theta^*=a_1(t)\cos(\pi x^*)\sin(\pi z^*)+d_1(t)\sin(2\pi z^*), \tag{4.2.7}$$

$$\Psi^*=b_1(t)\sin(\pi x^*)\sin(\pi z^*) \tag{4.2.8}$$

and

$$\sigma^*=c_1(t)\cos(\pi x^*)\sin(\pi z^*)+e_1(t)\sin(2\pi z^*). \tag{4.2.9}$$

These extended solutions will not exactly satisfy the non-linear equations, because the Galerkin approach is approximated. Substituting these proposed solutions (4.2.7) – (4.2.9) into the equations (4.2.1), (4.2.2) and (4.2.3), and performing the Galerkin projection where the coefficients of $\sin(\pi z^*)$ and that of $\sin(2\pi z^*)$ are required to vanish, and ignoring the higher harmonics, we have the respective equations as

$$a_1(t)+2\pi b_1(t)-\frac{\beta\Delta S}{\alpha\Delta T}c_1(t)=0, \tag{4.2.10}$$

$$M\dot{a}_1(t)+Ra\pi^2b_1(t)d_1(t)+Ra\pi b_1(t)+2\pi^2a_1(t)=0, \tag{4.2.11}$$

$$\dot{d}_1(t)-Ra\frac{\pi^2}{2}a_1(t)b_1(t)+4\pi^2d_1(t)=0, \tag{4.2.12}$$

$$\dot{c}_1(t) + \frac{Ra}{\phi}\pi^2 b_1(t)e_1(t) + \frac{Ra}{\phi}\pi b_1(t) + 2Le\pi^2 c_1(t) = 0, \tag{4.2.13}$$

and

$$\dot{e}_1(t) - \frac{\pi^2}{2}\frac{Ra}{\phi}b_1(t)c_1(t) + 4Le\pi^2 e_1(t) = 0. \tag{4.2.14}$$

For the steady state, the first derivatives are zero, and so we have the set of equations

$$a_1(t) + 2\pi b_1(t) - \frac{\beta\Delta S}{\alpha\Delta T}c_1(t) = 0, \tag{4.2.15}$$

$$Ra\pi^2 b_1(t)d_1(t) + Ra\pi b_1(t) + 2\pi^2 a_1(t) = 0, \tag{4.2.16}$$

$$-Ra\frac{\pi^2}{2}a_1(t)b_1(t) + 4\pi^2 d_1(t) = 0, \tag{4.2.17}$$

$$\frac{Ra}{\phi}\pi^2 b_1(t)e_1(t) + \frac{Ra}{\phi}\pi b_1(t) + 2Le\pi^2 c_1(t) = 0, \tag{4.2.18}$$

and

$$-\frac{\pi^2}{2}\frac{Ra}{\phi}b_1(t)c_1(t) + 4Le\pi^2 e_1(t) = 0. \tag{4.2.19}$$

From equation (4.2.15), we have the value of a_1 as

$$a_1 = -2\pi b_1 + \frac{\beta\Delta S}{\alpha\Delta T}c_1. \tag{4.2.20}$$

Putting this value of a_1 in equation (4.2.16), we have

$$Ra\pi^2 b_1 d_1 + Ra\pi b_1 - 4\pi^3 b_1 + 2\pi^2\frac{\beta\Delta S}{\alpha\Delta T}c_1 = 0. \tag{4.2.21}$$

Putting a_1 in equation (4.2.17), we have the value of d_1 as

$$d_1 = -\frac{\pi Ra}{4}b_1^2 + \frac{Ra_s}{8}b_1 c_1. \tag{4.2.22}$$

Put this value of d_1 in equation (4.2.21), we have c_1 as

$$c_1 = \frac{2Ra\left(Ra^2\pi^2 b_1^3 - 4\left(Ra - 4\pi^2\right)b_1\right)}{Ra^2 Ra_s\pi b_1^2 + 16\pi Ra_s}. \tag{4.2.23}$$

From equation (4.2.19), we have

$$e_1 = \frac{Ra}{8\pi Le\phi}b_1 c_1. \tag{4.2.24}$$

Put c_1 in equation (4.2.24), we have

$$e_1 = \frac{Ra}{8\pi Le\phi}b_1\left(\frac{2Ra\left(Ra^2\pi^2 b_1^3 - 4\left(Ra - 4\pi^2\right)b_1\right)}{Ra^2 Ra_s\pi b_1^2 + 16\pi Ra_s}\right). \tag{4.2.25}$$

Put the values of c_1 and e_1 in equation (4.2.18), we have a polynomial in b_1 as follows

$$b_1\left(Ab_1^4 + Bb_1^2 + C\right) = 0, \tag{4.2.26}$$

where

$$A = Ra^5\pi^4, \tag{4.2.27}$$

$$B = -4Ra^3\pi^2\left(Ra - 4\pi^2\right) + 4LeRa^3Ra_s\pi^2\phi + 16Le^2\phi^2\pi^4Ra^3, \tag{4.2.28}$$

and

$$C = 64\pi^2\phi LeRaRa_s - 64Le^2\phi^2\pi^2Ra\left(Ra - 4\pi^2\right). \tag{4.2.29}$$

The critical Rayleigh number Ra^c is calculated by setting $C = 0$,

$$64\pi^2\phi LeRaRa_s - 64Le^2\phi^2\pi^2Ra\left(Ra - 4\pi^2\right) = 0. \tag{4.2.30}$$

Solving this for Ra, we get the critical Rayleigh number Ra^c to be

$$Ra^c = 4\pi^2 + \frac{Ra_s}{Le\phi}. \tag{4.2.31}$$

This is the same as what we found in section 4.1, in the equation (4.1.49).

4.2.1 Bifurcation diagrams for steady state.

The polynomial in equation (4.2.26), has the variable b_1 which is the coefficient of the stream-function that gives the velocity components. The polynomial has two factors: the first one on the left corresponds to the base state $b_1 = 0$. The second factor is a quadratic and its solution is

$$b_1^2 = -\frac{B}{2A} \pm \frac{\sqrt{B^2 - 4AC}}{2A}. \tag{4.2.32}$$

If $B > 0$ and $C < 0$ so that $B^2 < 4AC$ is satisfied, we have only one positive real solution for b_1^2, which implies that we have two solutions for b_1 additional to the trivial solution. We have three solutions indeed. If $C > 0$, then there is no real solution for b_1 except the trivial solution. Hence at the point $C = 0$, the number of real solutions for b_1 changes.

If $B < 0$ and $C > 0$ but $B^2 - 4AC > 0$, there are two positive real solutions for b_1^2, which implies four solutions for b_1 additional to the trivial one of $b_1 = 0$. So we have five solutions. If $C < 0$, there is no real solution except the trivial one. This says that when $C = 0$, the number of solutions changes. In dynamical system, we call such a point a bifurcation point. The diagrams showing the bifurcations in double-diffusive convection are presented in Figure 4.9 and Figure 4.10.

In Figure 4.9, the amplitude b_1 is plotted against the Rayleigh number Ra for $Ra_s = -5$. At the point D, there is a supercritical pitchfork bifurcation at the critical value $Ra^c \simeq -160.521$. At this point two important things happen, the first one is that the number of solutions changes from one to three. The second one is that the stability of the base state changes from stable to unstable. The amplitude of the stream-function and that of flow field are increasing from the bifurcation point D.

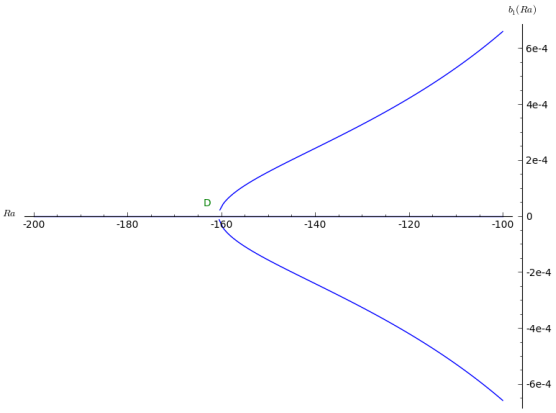

Figure 4.9: Bifurcation for b_1, an amplitude for stream function as function of Ra, when $Ra_s = -5$ and $Ra^c \simeq -160.521$.

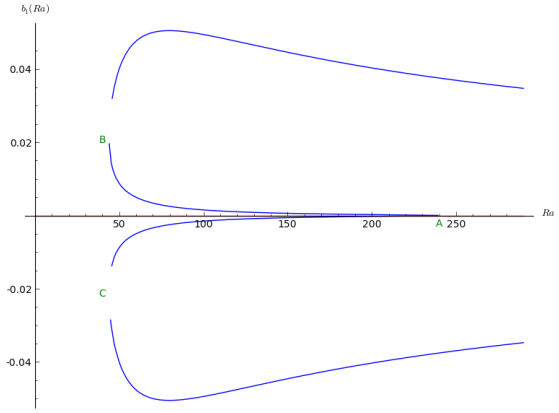

Figure 4.10: Bifurcation for b_1, an amplitude for stream function as function of Ra, when $Ra_s = 5$ and $Ra^c \simeq 239.478$.

In Figure 4.10, the amplitude b_1 is plotted against the Rayleigh number Ra for $Ra_s = 5$. At the point A, there is a sub-critical pitchfork bifurcation where below the critical value $Ra^c \simeq 239.478$ there are five solutions but after that point the solutions reduce to three, because there are three solutions which merge to give one solution. There are two symmetric saddle-node bifurcation at point B and at point C, the solutions are split into two.

The amplitude of stream function and that of flow field are finite since the growth after point B and after point C became steady. This is happening when $B^2 - 4AC = 0$, which correspond to $Ra \simeq 44.915$. The Rayleigh number corresponding to the stability boundary for base state which was obtained using linear stability analysis (see equation (4.1.50)), is at $Ra \simeq 51.452$.

4.2.2 Numerical method for non-steady state.

We obtain the value of $b_1(t)$ from equation (4.2.10), as

$$b_1(t) = -\frac{a_1(t)}{2\pi} + \frac{Ra_s}{2\pi Ra} c_1(t). \tag{4.2.33}$$

We substituted the equation (4.2.33) in equations (4.2.11), (4.2.12),(4.2.13) and (4.2.14) to have the following system of first order differential equations in time.

$$\dot{a}_1(t) = \frac{\pi Ra}{2M} a_1(t) d_1(t) - \frac{\pi Ra_s}{2M} c_1(t) d_1(t) + \frac{(Ra - 4\pi^2)}{2M} a_1(t) - \frac{Ra_s}{2M} c_1(t), \tag{4.2.34}$$

$$\dot{c}_1(t) = \frac{\pi Ra}{2\phi} a_1(t) e_1(t) - \frac{\pi Ra_s}{2\phi} c_1(t) e_1(t) + \frac{Ra}{2\phi} a_1(t) - \left(\frac{Ra_s}{2\phi} + 2\pi^2 Le \right) c_1(t), \tag{4.2.35}$$

$$\dot{d}_1(t) = -\frac{\pi Ra}{4} a_1^2(t) + \frac{\pi Ra_s}{4} a_1(t) c_1(t) - 4\pi^2 d_1(t), \tag{4.2.36}$$

and

$$\dot{e}_1(t) = -\frac{\pi Ra}{4\phi} a_1(t) c_1(t) + \frac{\pi Ra_s}{4\phi} c_1^2(t) - 4Le\pi^2 e_1(t). \tag{4.2.37}$$

After fixing the parameters M, ϕ and Le, we solved numerically the equations (4.2.34), (4.2.35), (4.2.36) and (4.2.37). We used $python$ where we have imported $odeint$ and ode from the package

$scipy.integrate$. We fixed the value of Ra_s to -5 or to 5 to be on the left hand part or right hand part of Figure 4.2. We took several values of Ra,(recall that to shift from negative to positive values implies moving from downward to upward of the same Figure 4.2), and we solved the above system of equations and we replaced $a_1(t)$ and $c_1(t)$ in equation (4.2.33) to get the stream function amplitude $b_1(t)$. The simulated values of $b_1(t)$ were plotted in each case.

The numerical experiments were performed by fixing the parameters. We changed the initial conditions and we have performed simulations respectively. Then we have observed the behaviour of the steady state solutions.

At $Ra_s = -5$ and $Ra = -170$, the base state is a global attractor because after changing slightly but not infinitesimal the initial conditions, the solution converges to the zero steady state (see Figures 4.11 and 4.12). This happens at the parameter Ra less than -160.521, the bifurcation point D (see Figure 4.9 for bifurcation information).

At $Ra_s = -5$ and $Ra = -158$, the base state is not a global attractor because after changing slightly but not infinitesimal the initial conditions, the solution converges to one non-zero steady state for Figure 4.13 and to another non-zero steady state (see Figure 4.14). Since the numerical solutions are converging to these non-zero steady states, they are stable but not global attractors. This happens at the parameter value Ra greater than -160.521, the bifurcation point D (see Figure 4.9 for bifurcation information).

At $Ra_s = 5$ and $Ra = 45$, the base state is stable because after changing slightly but not infinitesimal the initial conditions, the solution converges to the zero steady state (see Figures 4.15 and 4.16). We have oscillatory convergence to the base state, as predicted by linear stability analysis.

At $Ra_s = 5$ and $Ra = 53$, the steady states are not globally attractive because after changing slightly but not infinitesimal the initial conditions, the solution converges to one non-zero steady state for Figure 4.17 and to another non-zero steady state for Figure 4.18. Since the numerical solutions are converging to these non-zero steady states, they are stable but not global attractors but they are symmetric: one positive; another negative.

At $Ra_s = 5$ and $Ra = 250$, the base state is not a global attractor because after changing slightly but not infinitesimal the initial conditions, the solution converges to non-zero steady state for Figure 4.19 and to another non-zero steady state for Figure 4.20). Since the numerical solutions are converging to these non-zero steady states, they are stable but not global attractors.

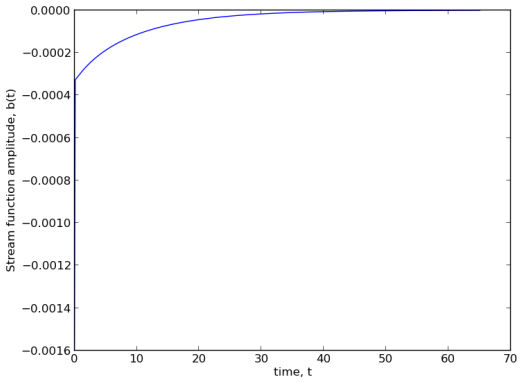

Figure 4.11: Amplitude for stream-function $b_1(t)$ as a function of time t, when $M = 0.5, \phi = 0.25, Le = 0.1$ $Ra_s = -5$ and $Ra = -170$ and initial conditions: $a_1(0) = 0.01, c_1(0) = 0.01, d_1(0) = 0$ and $e_1(0) = 0$.

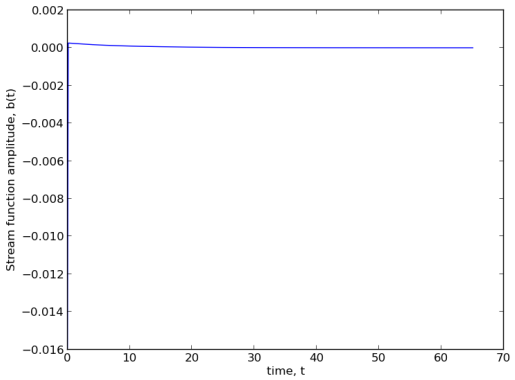

Figure 4.12: Amplitude for stream-function $b_1(t)$ as a function of time t, when $M = 0.5, \phi = 0.25, Le = 0.1$ $Ra_s = -5$ and $Ra = -170$ and initial conditions: $a_1(0) = 0.1, c_1(0) = 0.1, d_1(0) = 0$ and $e_1(0) = 0$.

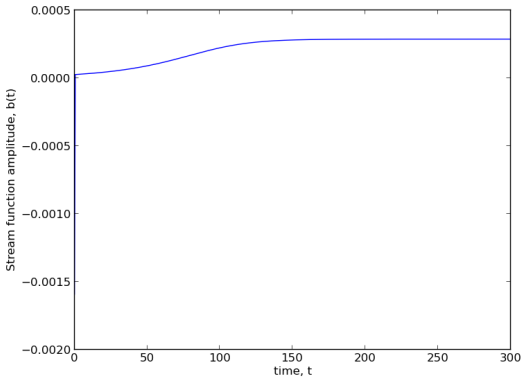

Figure 4.13: Amplitude for stream-function $b_1(t)$ as a function of time t, when $M = 0.5, \phi = 0.25, Le = 0.1$ $Ra_s = -5$ and $Ra = -158$ and initial conditions: $a_1(0) = 0.01, c_1(0) = 0.01, d_1(0) = 0$ and $e_1(0) = 0$.

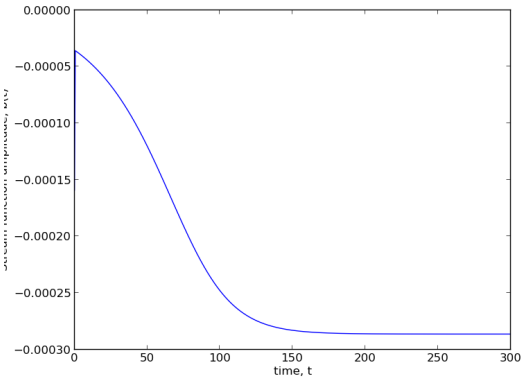

Figure 4.14: Amplitude for stream-function $b_1(t)$ as a function of time t, when $M = 0.5, \phi = 0.25, Le = 0.1$ $Ra_s = -5$ and $Ra = -158$ and initial conditions: $a_1(0) = 0.001, c_1(0) = 0.01, d_1(0) = 0$ and $e_1(0) = 0$.

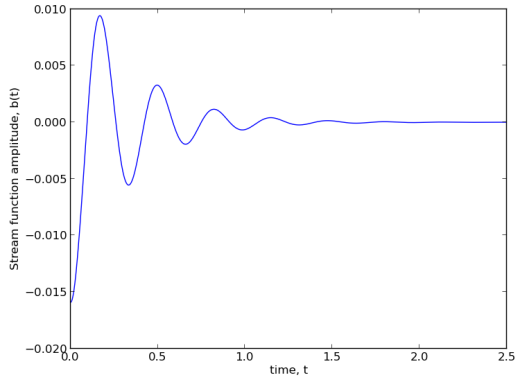

Figure 4.15: Amplitude for stream-function $b_1(t)$ as a function of time t, when $M = 0.5, \phi = 0.25, Le = 0.1$ $Ra_s = 5$ and $Ra = 45$ and initial conditions: $a_1(0) = 0.1, c_1(0) = 0.1, d_1(0) = 0$ and $e_1(0) = 0$.

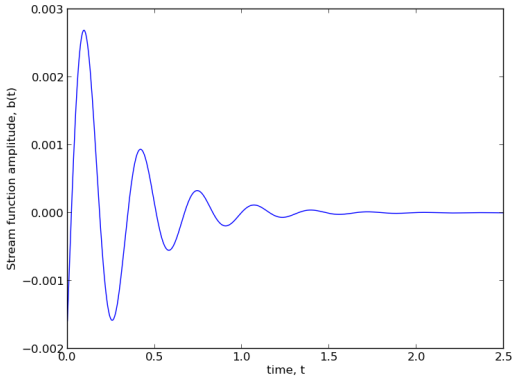

Figure 4.16: Amplitude for stream-function $b_1(t)$ as a function of time t, when $M = 0.5, \phi = 0.25, Le = 0.1$ $Ra_s = 5$ and $Ra = 45$ and initial conditions: $a_1(0) = 0.01, c_1(0) = 0.1, d_1(0) = 0$ and $e_1(0) = 0$.

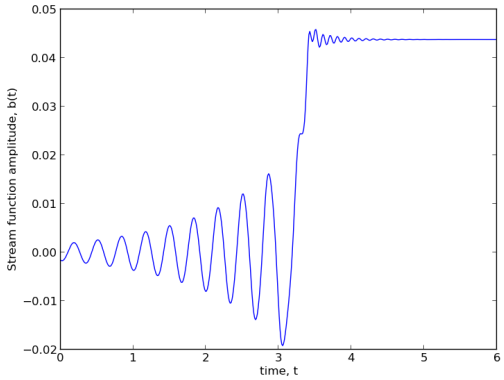

Figure 4.17: Amplitude for stream-function $b_1(t)$ as a function of time t, when $M = 0.5, \phi = 0.25, Le = 0.1$ $Ra_s = 5$ and $Ra = 53$ and initial conditions: $a_1(0) = 0.01, c_1(0) = 0.01, d_1(0) = 0$ and $e_1(0) = 0$.

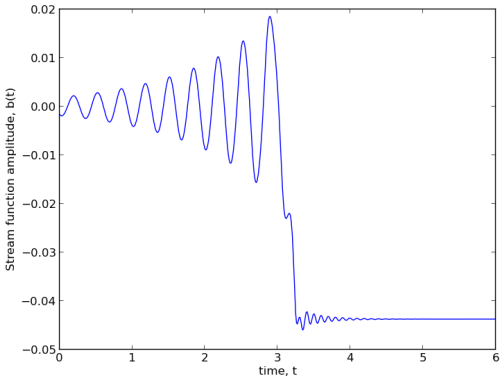

Figure 4.18: Amplitude for stream-function $b_1(t)$ as a function of time t, when $M = 0.5, \phi = 0.25, Le = 0.1$ $Ra_s = 5$ and $Ra = 53$ and initial conditions: $a_1(0) = 0.01, c_1(0) = 0.001, d_1(0) = 0$ and $e_1(0) = 0$.

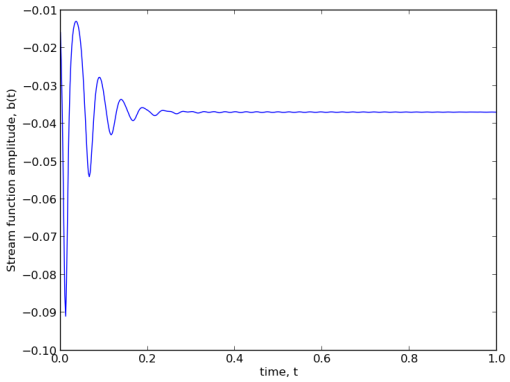

Figure 4.19: Amplitude for stream-function $b_1(t)$ as a function of time t, when $M = 0.5, \phi = 0.25, Le = 0.1$ $Ra_s = 5$ and $Ra = 250$ and initial conditions: $a_1(0) = 0.1, c_1(0) = 0.1, d_1(0) = 0$ and $e_1(0) = 0$.

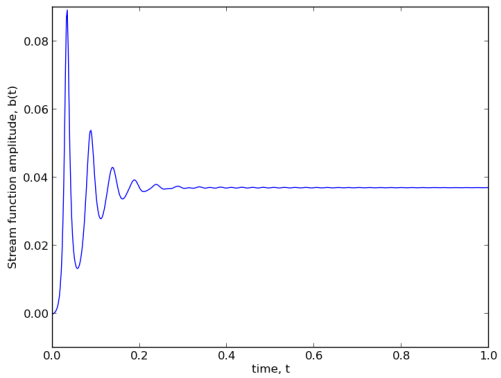

Figure 4.20: Amplitude for stream-function $b_1(t)$ as a function of time t, when $M = 0.5, \phi = 0.25, Le = 0.1$ $Ra_s = 5$ and $Ra = 250$ and initial conditions: $a_1(0) = 0.001, c_1(0) = 0.1, d_1(0) = 0$ and $e_1(0) = 0$.

5. Conclusion and Recommendations

Thermal convection was analysed, where we have applied linear perturbation theory on governing equations. From the dispersion relation, we obtained the critical value for the Rayleigh number. The stability analysis was carried out and we found that the perturbations below this critical value decay and those above this value grow. In the thermal convection the diffusion and buoyancy were competing. Locally, at any point in the layer, if temperature is relatively high then there is upward flow, and if temperature is relatively low then there is downward flow.

Both temperature and salinity gradients were taken into account for double-diffusive convection. The linear stability analysis was used and shows that there are two stability boundaries. When the system was crossing one boundary, the salinity gradient was negative and the perturbations grew exponentially: this happens when hot salty water overlies cold fresh water. When the system crossed the other boundary, the salinity gradient was positive. The perturbations were oscillatory: this happens when cold fresh water overlies hot salty water. The oscillations decayed or grew depending on whether the system was in the stable region or in unstable region respectively.

In double-diffusive convection, there was a competition between temperature and salt concentration gradients in the sense that locally, at any point in the layer, a positive perturbation to temperature tended to cause upflow, while a positive perturbation to salinity tend to cause downflow. Globally in the first quadrant, if the temperature gradient wins, then there will be motion (both upward and downward in different places), while if the salinity gradient wins, then the motion will decay over time. In the third quadrant, if the temperature gradient wins the motion will grow exponentially while if the salinity gradient wins, then the motion will decay exponentially.

The non-linear analysis was studied using Galerkin approximation method. We found that the perturbations do not grow forever. They saturated at finite amplitudes. The performed numerical experiments showed that when the initial conditions change in the stable region, the solutions converge to the base steady state solution (which implies that they converge at zero amplitude) and that the steady base state is a global attractor. But in the unstable region, when the initial conditions change, the solutions converge to non-zero steady states, and when parameters continue to change, the value of the non-zero amplitude also changes.

The possible further research directions include the study of the behaviour of the system at higher Rayleigh numbers where weakly non-linear approach is no longer valid. Here the suggested approach is to use the singular perturbation theory (see section 14.9 of Fowler (1997)). The other one is to investigate the effect of reactions that involve the behaviour of the temperature, salinity and the porosity (see Pritchard and Richardson (2007) and Corson (2012)).

AppendixA. The figures completing the cycle

We have presented in the main work some figures for half cycle (from 0 to $\pi/4$) and here we list the other figures (from $\pi/2$ to π) and the figures for the next half cycle (from $5\pi/4$ to 2π) their interpretations are present in subsection 4.1.4.

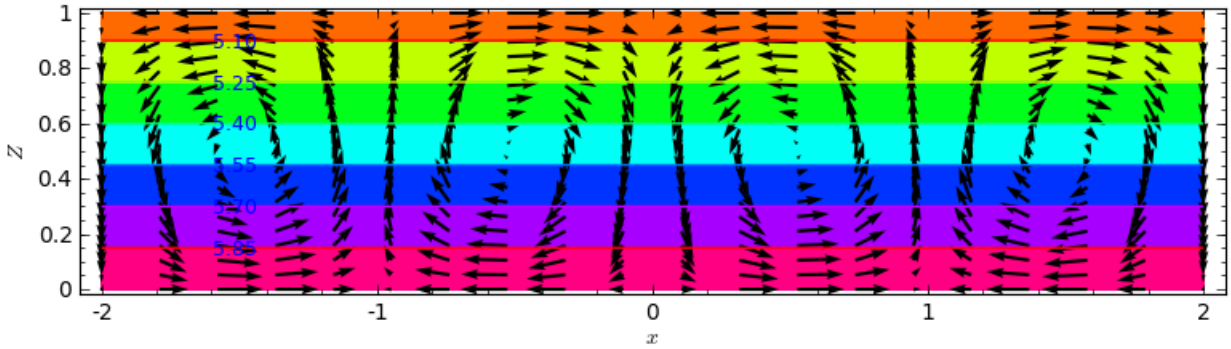

Figure A.1: From first quadrant, the orange color at the top for low and pink at the bottom for high temperature and velocity field for $\epsilon = 0.025$, $Ra_s = 5$, $Ra = 51.542$, $\phi = 0.25$, $Le = 0.1$ and $M = 0.5$; at $n_i t^* = \pi/2$, for $x = 0$, maximum scaled velocity $\simeq -8.340$ at $z = 0.5$.

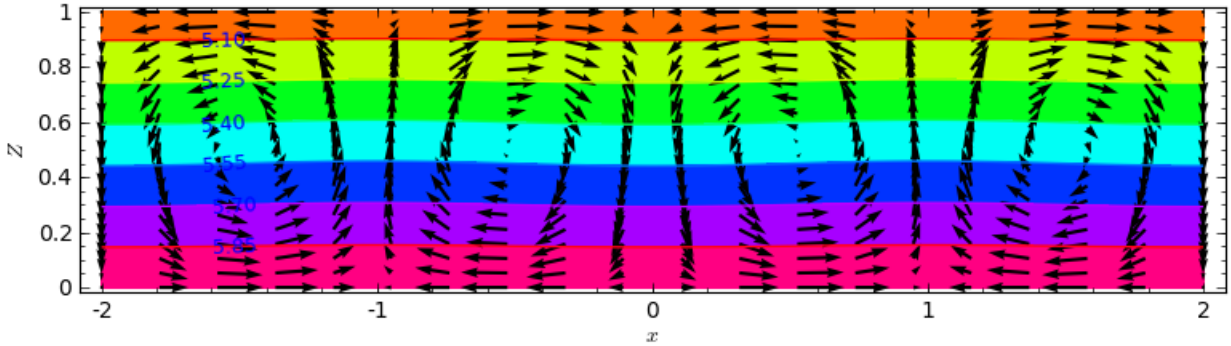

Figure A.2: From first quadrant, the orange color at the top for low and pink at the bottom for high concentration and velocity field, for $\epsilon = 0.025$, $Ra_s = 5$, $Ra = 51.542$, $\phi = 0.25$, $Le = 0.1$ and $M = 0.5$; at $n_i t^* = \pi/2$, for $x = 0$, maximum scaled velocity $\simeq -8.340$ at $z = 0.5$.

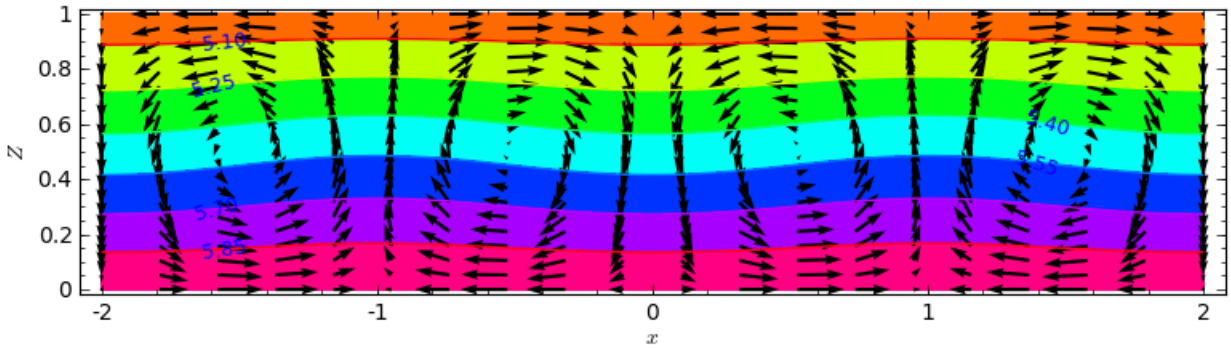

Figure A.3: From first quadrant, the orange color at the top for low and pink at the bottom for high temperature and velocity field for $\epsilon = 0.025$, $Ra_s = 5$, $Ra = 51.542$, $\phi = 0.25$, $Le = 0.1$ and $M = 0.5$; at $n_i t^* = 3\pi/4$, for $x = 0$, maximum scaled velocity $\simeq -6.440$ at $z = 0.5$

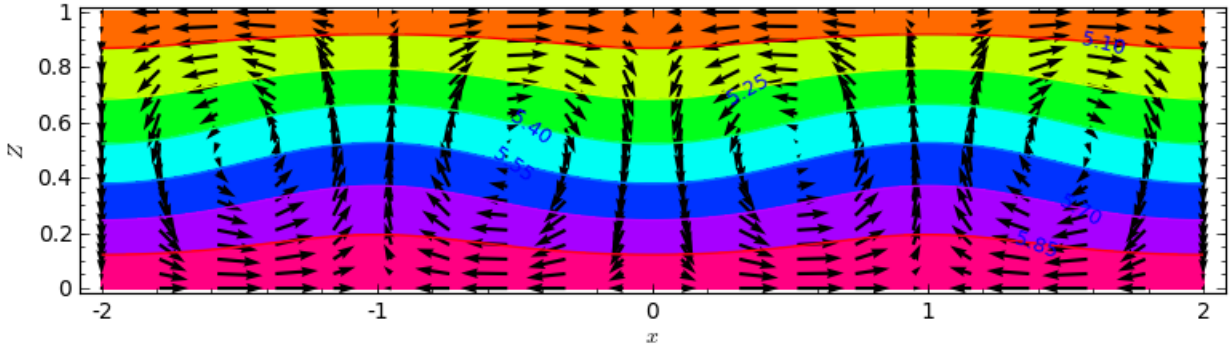

Figure A.4: From first quadrant, the orange color at the top for low and pink at the bottom for high concentration and velocity field, for $\epsilon = 0.025$, $Ra_s = 5$, $Ra = 51.542$, $\phi = 0.25$, $Le = 0.1$ and $M = 0.5$; at $n_i t^* = 3\pi/4$, for $x = 0$, maximum scaled velocity $\simeq -6.440$ at $z = 0.5$.

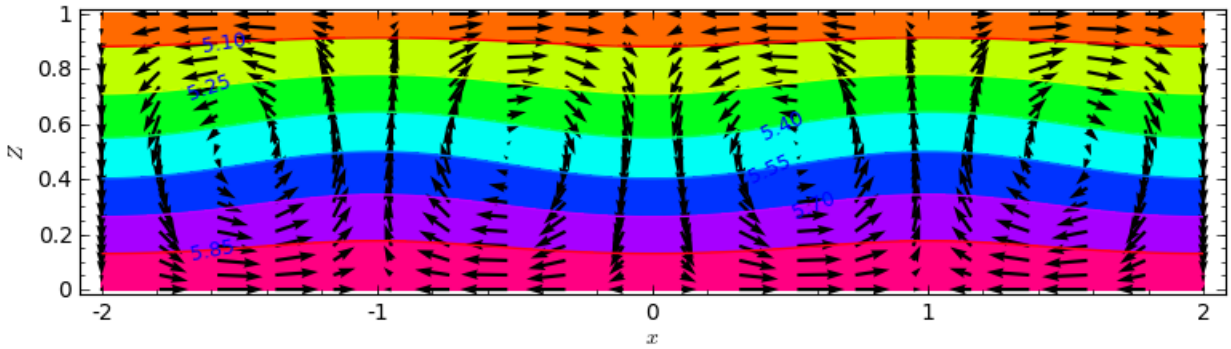

Figure A.5: From first quadrant, the orange color at the top for low and pink at the bottom for high temperature and velocity field for $\epsilon = 0.025$, $Ra_s = 5$, $Ra = 51.542$, $\phi = 0.25$, $Le = 0.1$ and $M = 0.5$; at $n_i t^* = \pi$, for $x = 0,$ maximum scaled velocity $\simeq -0.767$ at $z = 0.5$.

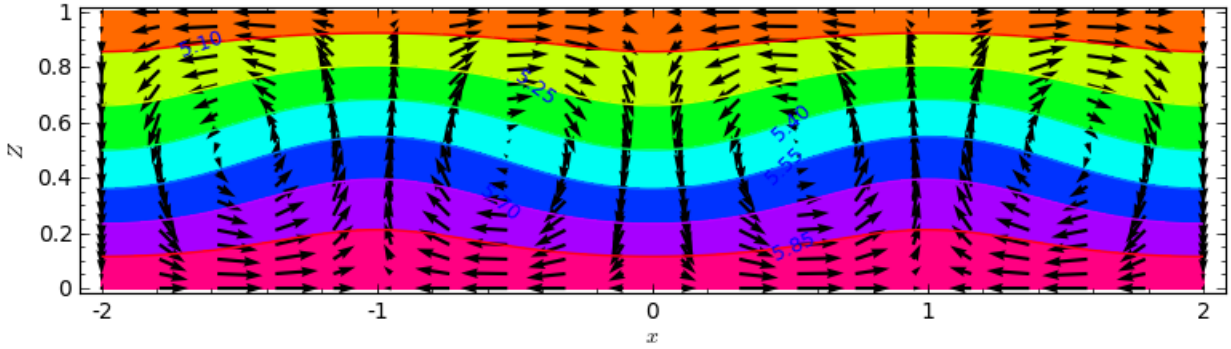

Figure A.6: From first quadrant, the orange color at the top for low and pink at the bottom for high concentration and velocity field, for $\epsilon = 0.025$, $Ra_s = 5$, $Ra = 51.542$, $\phi = 0.25$, $Le = 0.1$ and $M = 0.5$; at $n_i t^* = \pi$, for $x = 0,$ maximum scaled velocity $\simeq -0.767$ at $z = 0.5$.

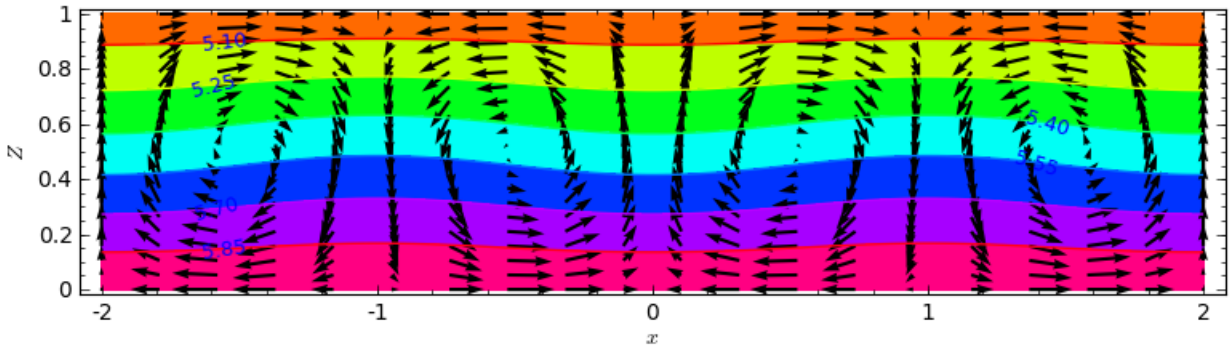

Figure A.7: From first quadrant, the orange color at the top for low and pink at the bottom for high temperature and velocity field for $\epsilon = 0.025$, $Ra_s = 5$, $Ra = 51.542$, $\phi = 0.25$, $Le = 0.1$ and $M = 0.5$; at $n_i t^* = 5\pi/4$, for $x = 0$, maximum scaled velocity $\simeq 5.355$ at $z = 0.5$.

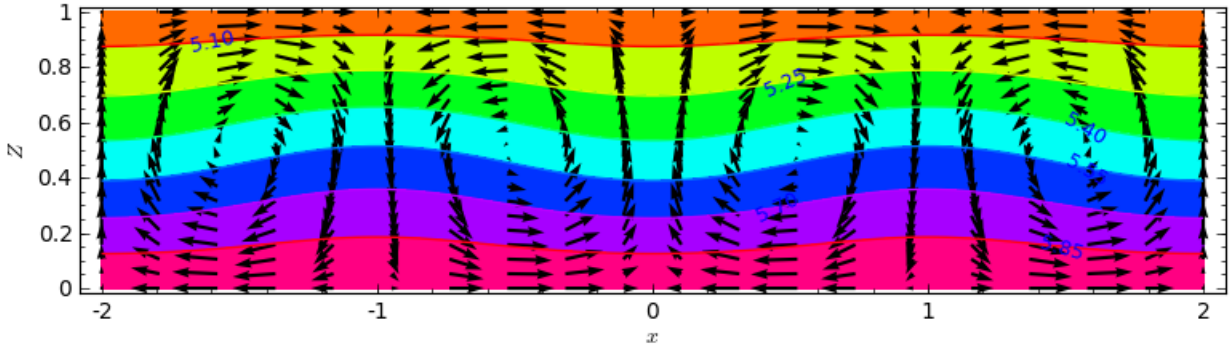

Figure A.8: From first quadrant, the orange color at the top for low and pink at the bottom for high concentration and velocity field, for $\epsilon = 0.025$, $Ra_s = 5$, $Ra = 51.542$, $\phi = 0.25$, $Le = 0.1$ and $M = 0.5$; at $n_i t^* = 5\pi/4$, for $x = 0$, maximum scaled velocity $\simeq 5.355$ at $z = 0.5$.

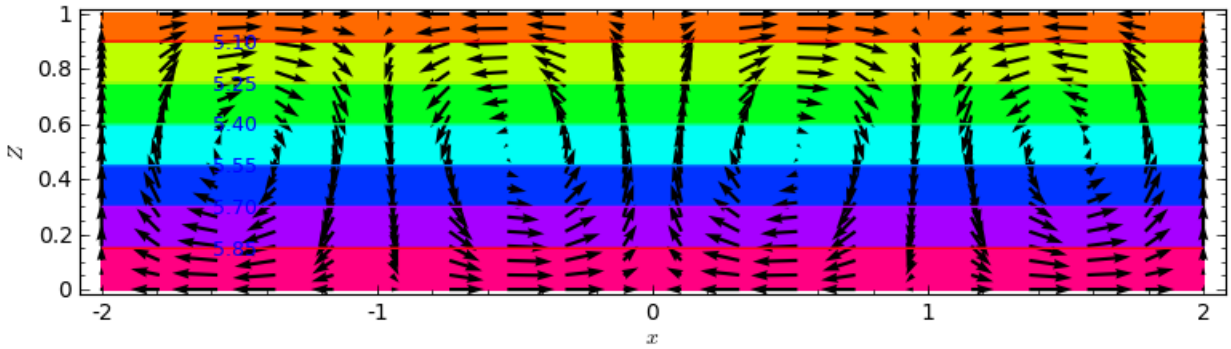

Figure A.9: From first quadrant, the orange color at the top for low and pink at the bottom for high temperature and velocity field for $\epsilon = 0.025$, $Ra_s = 5$, $Ra = 51.542$, $\phi = 0.25$, $Le = 0.1$ and $M = 0.5$; at $n_i t^* = 3\pi/2$, for $x = 0$, maximum scaled velocity $\simeq 8.340$ at $z = 0.5$.

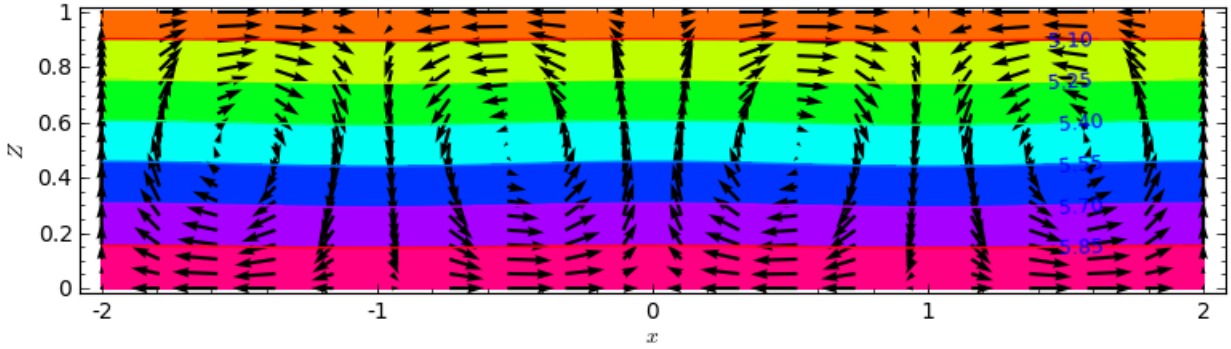

Figure A.10: From first quadrant, the orange color at the top for low and pink at the bottom for high concentration and velocity field, for $\epsilon = 0.025$, $Ra_s = 5$, $Ra = 51.542$, $\phi = 0.25$, $Le = 0.1$ and $M = 0.5$; at $n_i t^* = 3\pi/2$, for $x = 0$, maximum scaled velocity $\simeq 8.340$ at $z = 0.5$.

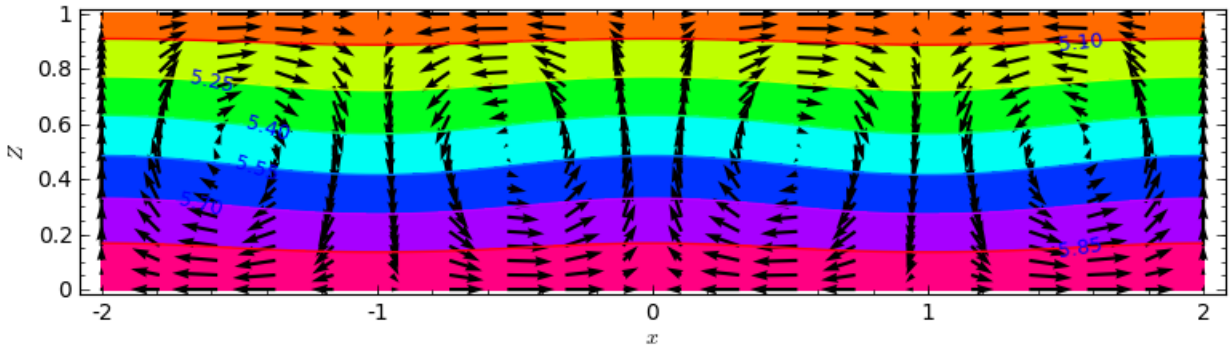

Figure A.11: From first quadrant, the orange color at the top for low and pink at the bottom for high temperature and velocity field for $\epsilon = 0.025$, $Ra_s = 5$, $Ra = 51.542$, $\phi = 0.25$, $Le = 0.1$ and $M = 0.5$; at $n_i t^* = 7\pi/4$, for $x = 0$, maximum scaled velocity $\simeq 6.440$ at $z = 0.5$.

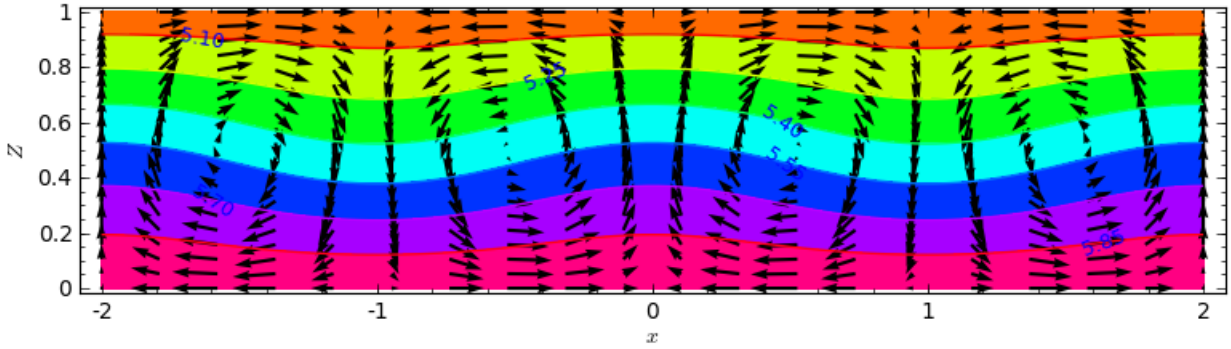

Figure A.12: From first quadrant, the orange color at the top for low and pink at the bottom for high concentration and velocity field, for $\epsilon = 0.025$, $Ra_s = 5$, $Ra = 51.542$, $\phi = 0.25$, $Le = 0.1$ and $M = 0.5$; at $n_i t^* = 7\pi/4$, for $x = 0$, maximum scaled velocity $\simeq 6.440$ at $z = 0.5$.

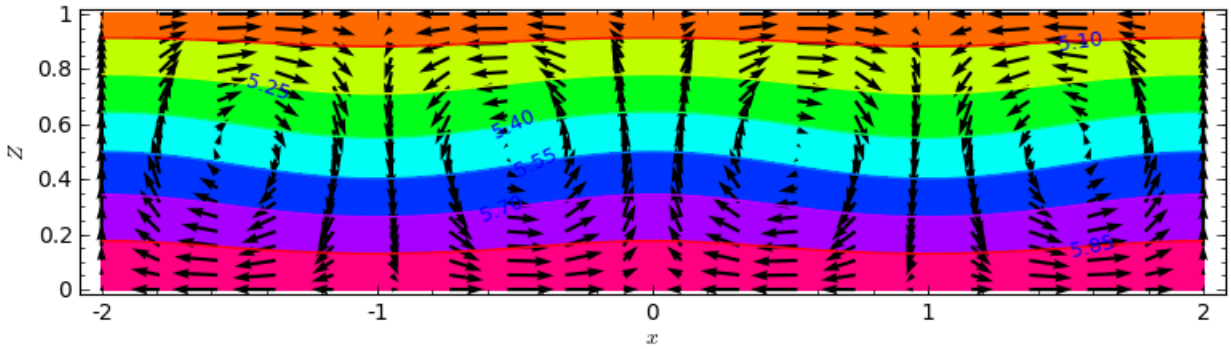

Figure A.13: From first quadrant, the orange color at the top for low and pink at the bottom for high temperature and velocity field for $\epsilon = 0.025$, $Ra_s = 5$, $Ra = 51.542$, $\phi = 0.25$, $Le = 0.1$ and $M = 0.5$; at $n_i t^* = 2\pi$, for $x = 0,$ maximum scaled velocity $\simeq 0.767$ at $z = 0.5$.

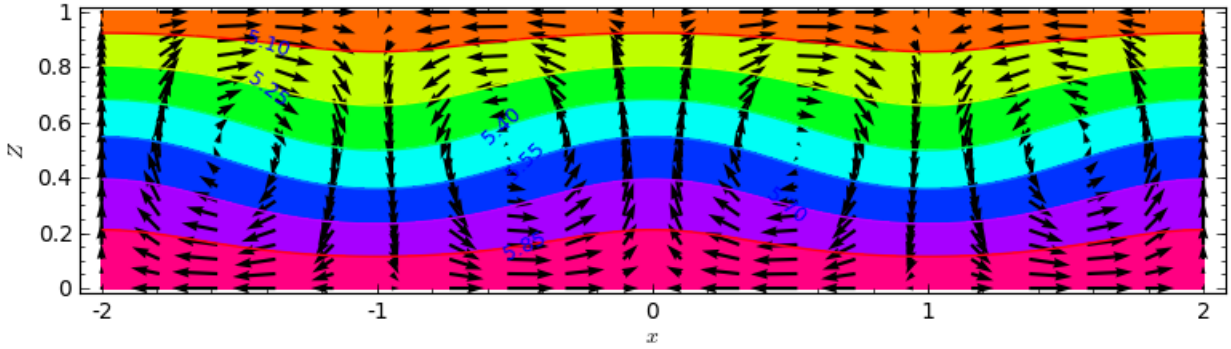

Figure A.14: From first quadrant, the orange color at the top for low and pink at the bottom for high concentration and velocity field, for $\epsilon = 0.025$, $Ra_s = 5$, $Ra = 51.542$, $\phi = 0.25$, $Le = 0.1$ and $M = 0.5$; at $n_i t^* = 2\pi$, for $x = 0,$ maximum scaled velocity $\simeq 0.767$ at $z = 0.5$.

References

Francois Charru. *Hydrodynamic Instabilities*. Cambridge University Press, 2011.

Lindsey T. Corson. *Geochemical Effects on Natural Convection in Porous Media*. PhD thesis, University of Strathclyde, Glasgow, U.K, 2012.

P.G. Drazin. *Introduction to Hydrodynamic Stability*. Cambridge University Press, 2002.

A.C. Fowler. *Mathematical Models in the Applied Sciences*. Cambridge University Press, 1997.

Claude Godreche and Paul Manneville. *Hydrodynamics and Nonlinear Instabilities*. Cambridge University Press, 1998.

C. W. Horton and F. T. Rogers. Convection currents in a porous medium. *Journal of Applied Physics*, 16:367–370, 1945.

Vinay Kumar. *Coupling of Free Flow and Flow in Porous Media-Dimensional Analysis and Numerical Investigation*. M.sc. thesis, University of Stuttgart, 2012.

Pijush K. Kundu, Ira M.Cohen, and David R.Dowling. *Fluid Mechanics (Fifth Edition)*. Academic Press, 2012.

E. R. Lapwood. Convection of a fluid in a porous medium. *Proc. Camb. Phil. Soc.*, 44:508–521, 1948.

M. Mamou and P. Vasseur. Thermosolutal bifurcation phenomena in porous enclosures subject to vertical temperature and concentration gradients. *J. Fluid Mech.*, 395:61–87, 1999.

Donald A. Nield and Adrian Bejan. *Convection in Porous Media (Third Edition)*. Springer, 2006.

F.J. O'Brien, B.A. Harley, M.A. Waller, I.V. Yannas, L.J. Gibson, and P.J. Prendergast. The effect of pore size on permeability and cell attachment in collagen scaffolds for tissue engineering. *Technology and Health Care*, 15:3–17, 2007.

Patrick H. Oosthuizen and David Naylor. *An Introduction to Convective Heat Transfer Analysis*. McGraw Hill, 1999.

Owen M . Phillips. *Geological Fluid Dynamics*. Cambridge University Press, 2009.

David Pritchard and Chris N. Richardson. The effect of temperature-dependant solubility on the onset of thermosolutal convection in a horizontal porous layer. *J. Fluid Mech.*, 571:59–95, 2007.

Steven H. Strogatz. *Nonlinear Dynamics and Chaos: With Applications to Physics, Biology, Chemistry and Engineering*. Westview Press, 1994.

Alexandru-Bogdan Tatomir. *Numerical Investigations of Flow through Fractured Porous Media*. M.sc. thesis, University of Stuttgart, 2007.

J. S. Turner. *Buoyancy Effects in Fluids*. Cambridge University Press, 1973.

M.G. Worster. *A Brief Introduction to Fluid Dynamics*. African Institute for Mathematical Sciences, 2008.